Monthly Notices
of the
ROYAL ASTRONOMICAL SOCIETY

MNRAS **461,** 1112–1129 (2016)
Advance Access publication 2016 May 26

doi:10.1093/mnras/stw1207

The evolution of galaxies at constant number density: a less biased view of star formation, quenching, and structural formation

Jamie R. Ownsworth,[1] Christopher J. Conselice,[1]★ Carl J. Mundy,[1] Alice Mortlock,[1,2] William G. Hartley,[1,3] Kenneth Duncan[1,4] and Omar Almaini[1]

[1]*University of Nottingham, School of Physics and Astronomy, Nottingham NG7 2RD, UK*
[2]*SUPA†, Institute for Astronomy, University of Edinburgh, Royal Observatory, Edinburgh EH9 3HJ, UK*
[3]*Institute for Astronomy, ETH Zurich, Wolfgang-Pauli-Strasse 27, CH-8093 Zurich, Switzerland*
[4]*Leiden Observatory, Leiden University, NL-2300 RA Leiden, Netherlands*

Accepted 2016 May 18. Received 2016 May 17; in original form 2015 June 29

ABSTRACT

Due to significant galaxy contamination and impurity in stellar mass selected samples (up to 95 per cent from $z = 0$–3), we examine the star formation history, quenching time-scales, and structural evolution of galaxies using a constant number density selection with data from the United Kingdom Infra-Red Deep Sky Survey Ultra-Deep Survey field. Using this methodology, we investigate the evolution of galaxies at a variety of number densities from $z = 0$–3. We find that samples chosen at number densities ranging from 3×10^{-4} to 10^{-5} galaxies Mpc^{-3} (corresponding to $z \sim 0.5$ stellar masses of $M_* = 10^{10.95-11.6}$ M$_0$) have a star-forming blue fraction of ∼50 per cent at $z \sim 2.5$, which evolves to a nearly 100 per cent quenched red and dead population by $z \sim 1$. We also see evidence for number density downsizing, such that the galaxies selected at the lowest densities (highest masses) become a homogeneous red population before those at higher number densities. Examining the evolution of the colours for these systems furthermore shows that the formation redshift of galaxies selected at these number densities is $z_{\rm form} > 3$. The structural evolution through size and Sérsic index fits reveal that while there remains evolution in terms of galaxies becoming larger and more concentrated in stellar mass at lower redshifts, the magnitude of the change is significantly smaller than for a mass-selected sample. We also find that changes in size and structure continues at $z < 1$, and is coupled strongly to passivity evolution. We conclude that galaxy structure is driving the quenching of galaxies, such that galaxies become concentrated before they become passive.

Key words: galaxies: evolution – galaxies: fundamental parameters – galaxies: high-redshift – galaxies: structure.

1 INTRODUCTION

In the local Universe, the most massive galaxies ($M_* > 10^{11}$ M$_\odot$) are a nearly homogeneous population. They have early-type morphologies, red rest-frame optical colours, and low star formation rates (SFRs; Bower, Lucey & Ellis 1992; Kauffmann et al. 2003; Gallazzi et al. 2005; Baldry et al. 2006; Conselice 2006b; Grützbauch et al. 2011; Ownsworth et al. 2012; Mortlock et al. 2013). A major unanswered question is: How have these massive galaxies evolved over cosmic time to become this population?

Recent measurements of the stellar mass function of galaxies out to $z = 4$ (e.g. Ilbert et al. 2013; Muzzin et al. 2013; Duncan et al. 2014; Mortlock et al. 2015) show evidence that significant numbers of massive galaxies exist at very early cosmic times. However, the total number densities of these massive galaxies grows substantially at later times, showing a drawn out formation history. By redshift $z \sim 1$, the number densities of massive galaxies with $M_* > 10^{11}$ M_0 are consistent with their $z = 0$ values, demonstrating a rapid formation within the first half of the universe's history (e.g. Conselice et al. 2007; Mortlock et al. 2011, 2015). This suggests that massive galaxies form some portion of their stellar mass very early in the universe, and then assemble the remainder of their mass very quickly.

Although the stellar mass functions of galaxies provide a simple and direct way to measure the abundance of a population and its overall growth as a function of time, it does not tell us how individual galaxies have assembled and evolved. Ultimately, one major goal is connecting local massive 'red and dead' galaxies to their progenitors

★ E-mail: conselice@nottingham.ac.uk
† Scottish Universities Physics Alliance.

at early cosmic times to examine how they evolved and changed in terms of their properties. However, connecting the same galaxies over cosmic time remains a significant problem that has yet to be fully resolved.

Over the last decade there has been extensive research into the evolution of massive galaxies. These studies have shown that the more massive a galaxy is today, the earlier its star formation and merging must have completed and subsided, and the earlier its morphology becomes spheroidal (e.g. Bundy, Ellis & Conselice 2005, Bundy et al. 2006; Renzini 2006; Conselice, Rajgor & Myers 2008; Mortlock et al. 2013). This is called 'Galaxy Downsizing', in which the most massive galaxies appear to be in place and stop forming in an apparently antihierarchical manner. At high redshift, massive galaxies also appear to be different from galaxies with the same stellar mass at lower redshifts. The massive high-z population consists of galaxies with low Sérsic indices, small sizes, and high star formation rates (e.g. Conselice et al. 2007; Daddi et al. 2007; Trujillo et al. 2007; Buitrago et al. 2008, 2013; Mortlock et al. 2013) compared with galaxies at similar masses in the low-z universe. However, these results are nearly all based on selecting galaxies at a constant stellar mass limit at all epochs, typically $\mathrm{M}_* > 10^{11}\ \mathrm{M}_0$.

However, Mundy, Conselice & Ownsworth (2015) recently showed that using a stellar mass limit such as $M_* > 10^{11}\ M_0$ leads to a significant precursor bias, such that the sample selected at low redshifts ($z \sim 0.5$) is 95 per cent contaminated with galaxies which were not in the sample at $z \sim 3$. This precursor bias gets even worse at higher redshifts. Using a constant number density selection reduces the precursor bias by a factor of at least 10 over using a constant stellar mass cut selection (Mundy et al. 2015). Mundy et al. (2015) find that while there is some contamination and incompleteness at the 50 per cent level, even when using a constant number density selection, the stellar mass and star formation properties remains the same to within a factor of 2. This is compared with the factors of >10 differences when using a stellar mass cut to trace the same star formation and average/total stellar masses within a selection (Mundy et al. 2015).

In this paper, we use constant number density selections to examine the evolutionary paths that distant massive galaxy progenitors have travelled to become the nearly homogeneous population we see today. With number density selection methods we aim to answer the questions: Do massive galaxies form in extreme star formation episodes in the early universe? At what cosmic epoch to they stop forming stars? How many galaxies evolve from the blue cloud to the red sequence? How has their structure changed from high redshift?

Recent work has begun to investigate the evolution of the properties of massive galaxies using number density techniques (e.g. Papovich et al. 2011; Conselice et al. 2013; Patel et al. 2013; Marchesini et al. 2014; Ownsworth et al. 2014; Papovich et al. 2015). Marchesini et al. (2014) showed using number density selections that the progenitors of ultramassive galaxies (selected with $\log M_* > 11.8$) appear to have red $U - V$ colours, but also host large amounts of star formation ($\mathrm{sSFR} > 10^{-10}\ \mathrm{yr}^{-1}$) at $z > 3$. They however find that the progenitors of ultramassive galaxies, including the star-forming objects, have never lived on the blue star-forming cloud in the last ~11 Gyr of cosmic history. Papovich et al. (2011) trace the star formation history of a luminosity based number density selection from high-z to low. In terms of galaxy formation, Conselice et al. (2013) investigate the gas accretion rate of a number density selected sample, and Ownsworth et al. (2014) calculate the relative contribution of minor and major mergers and gas accretion to galaxy formation within number density selected samples at $z < 3$.

Despite the importance of this approach, a general study examining the evolution of the most basic processes of galaxy formation – star formation histories, quenching, and the assembly of structure through time has not yet been done. In this paper, we investigate the evolution of galaxies with cosmic time of the progenitors of local massive galaxies with number volume densities from $n = 3 \times 10^{-4}\ \mathrm{Mpc}^{-3}$, to $n = 10^{-5}\ \mathrm{Mpc}^{-3}$ (corresponding to a mass limit of $M_* > 10^{10.95}\ M_0$ at $z = 0.5$) from $z = 3$ to 0. We use data from the United Kingdom Infra-Red Deep Sky Survey (UKIDSS) Ultra Deep Survey (UDS) to investigate this question, utilizing the DR8 release with a 5σ depth of $K = 24.6$ over $0.77\ \mathrm{deg}^2$.

We investigate the evolution of our sample's colours, stellar masses, SFRs, passivity, and structural parameters over the redshift range of $0.3 < z < 3.0$. We furthermore discuss how these characteristics change as a function of the initial comoving density. This is a companion paper to Ownsworth et al. (2014) where we investigate the merging history of the same galaxies through their mass assembly.

Throughout this paper we assume the cosmology $\Omega_\mathrm{M} = 0.3$, $\Omega_\lambda = 0.7$, and $H_0 = 70\,\mathrm{km\,s}^{-1}\ \mathrm{Mpc}^{-1}$. AB magnitudes and a Chabrier initial mass function (IMF) are used throughout. This paper is divided into the following sections. Section 2 discusses the data we use to carry out this analysis, including how we measure redshifts and stellar masses, and how we carry out our galaxy selection, Section 3 describes the results of the paper, and Section 4 is the summary.

2 DATA AND ANALYSIS

2.1 The UDS field

This work is based on the 8th data release (DR8) of the UDS (Almaini et al. in preparation), which is the deepest of the UKIRT (United Kingdom Infra-Red Telescope) UKIDSS (Lawrence et al. 2007) projects. The UDS covers $0.77\ \mathrm{deg}^2$ in the J, H, K bands and the limiting magnitudes (AB), within an aperture of 2 arcsec at the 5σ level, are 24.9, 24.2, 24.6 in J, H, K, respectively. It is the deepest infrared survey ever undertaken over such a large area at these wavelengths. It benefits from an array of ancillary multiwavelength data: U-band data from CFHT Megacam, B, V, R, i', and z'-band data from the Subaru–*XMM* Deep Survey (Furusawa et al. 2008); infrared data from the Spitzer Legacy Program (SpUDS). All of these are fundamental for the computation of accurate photometric redshifts, stellar masses, and rest-frame magnitudes (e.g. Hartley et al. 2013; Mortlock et al. 2015).

The galaxy catalogue employed in this work is K-band selected and contains approximately 96 000 galaxies. As mentioned, this survey reaches a depth of $K_{AB} = 24.6$ (5σ AB), which was determined from simulations and guarantees a 99 per cent completeness level (see Hartley et al. 2013 for more details). The depth and wavelength of the UDS allows us to study the distant Universe with fewer biases against red and dusty galaxies, which could otherwise be completely missed in ultraviolet and optical surveys.

2.2 Redshifts

The redshifts we use are a mixture of both photometric and spectroscopic redshifts. The spectroscopic redshifts we utilize are from the UDSz redshift survey (e.g. Hartley et al. 2013; Almaini et al., in preparation). The spectroscopic redshifts from UDSz (ESO 180.A-0776) are measured through fitting templates to the spectra and using the best-fitting template for the redshift. We however only use

spectra with a high certainty of having an accurate redshift measurement based on multiple emission lines or absorption features in the rest-frame UV (Almaini et al. in preparation). A further description of these redshifts is provided in Hartley et al. (2013). In total there are ∼1500 spectroscopic redshifts in this programme.

In addition to the redshifts from UDSz and other previous more focused programmes (see Hartley et al. 2015), we calculate photometric redshifts for our sample. We use these photometric redshifts by fitting template spectra to photometry using EAZY (Brammer, van Dokkum & Coppi 2008). The template fitting we use is done with the standard six EAZY templates and an extra blue one. This blue template is a combination of the bluest EAZY template and a small amount of SMC-like extinction using $A_V = 0.1$ and the SMC dust extinction law (Prevot et al. 1984). From inspection of UV spectra of $z > 2$ galaxies we determine that this slightly altered template does a better job of fitting some of these distant star-forming galaxies. We also used an interactive approach to determine the slight offsets in zero-points for our photometric bands to improve the agreements between the photometric and spectroscopic redshifts. Ultimately the photo-zs that we calculate from EAZY are based on the maximum likelihood redshift after taking into account the K-band apparent magnitude prior.

We tested our photometric redshifts for quality in a few ways. Our basis for measuring the photometric redshift quality is through comparing with the ∼1500 spectroscopic redshifts from UDSz and ∼4000 archival spectroscopic redshifts. After we remove obvious AGN and catastrophic outliers ($\delta z/(1+z) > 0.15$), we calculate that the dispersion between the photometric and the spectroscopic redshifts is $\delta z/(1+z) \sim 0.031$ (Hartley et al. 2013). Furthermore we performed the test of using close pairs of galaxies as outlined in Quadri & Williams (2010). The idea here is that galaxies which are close together on the sky are likely to be at similar redshifts (see also Hartley et al. 2013). We test our photo-zs with this method and find a similar photo-z quality as given by the comparison with spectroscopic redshifts.

2.3 Stellar masses and SED fitting

The stellar masses and rest-frame colours (UVJ) of our sample are measured using a multicolour stellar population fitting technique. For a full description see Mortlock et al. (2013) and Hartley et al. (2013). We fit synthetic spectral energy distributions (SEDs) constructed from the stellar populations models of Bruzual & Charlot (2003) to the U, B, V, R, i', z', J, H, K bands and IRAC channels 1 and 2, assuming a Chabrier IMF. The star formation history is characterized by an exponentially declining model with various ages, metallicity, and dust contents of the form

$$\mathrm{SFR}(t = \mathrm{obs}) = \mathrm{SFR_{form}} \times \exp(-\mathrm{t}/\tau), \quad (1)$$

where the values of the fitted τ ranges between 0.01 and 13.7 Gyr, and the age of the onset of star formation ranges from 0.001 to 13.7 Gyr. We exclude templates that are older than the age of the Universe at the redshift of the galaxy being fit. This declining SFR is well justified by previous work showing that the observed SFR indeed declines exponentially at the galaxy comoving densities we use in this paper (Ownsworth et al. 2014).

The metallicity used within the fitting ranges from 0.0001 to solar, and the dust content is parametrized, following Charlot & Fall (2000), by τ_v, the effective V-band optical depth. We use values up to $\tau_v = 2.5$ with a constant interstellar medium fraction of 0.3.

We fit our SEDs by first scaling the template K-band apparent magnitude to the observed galaxy K-band apparent magnitude. We then fit each scaled model template in the grid of SEDs to the measured photometry of each individual galaxy. We then calculate χ^2 values for each template, and select the best-fitting template, obtaining a corresponding stellar mass and rest-frame luminosities.

Hartley et al. (2013), following the method from Pozzetti et al. (2010), found the UDS 95 per cent mass completeness limit as a function of redshift given by: $\log M_{\mathrm{lim}} = 8.27 + 0.81z - 0.07z^2$. Galaxies that fall below M_{lim} are not used in the subsequent analysis. We base our measured densities on the stellar mass functions from Mortlock et al. (2015, Table 1). The resulting stellar mass limits for our study at the various number density selections are listed in Table 2. Our selections are similar to the mass range used in the study of Papovich et al. (2015) who examine the properties of the progenitors of galaxies with MW and M31 masses. Although we do not probe masses as low as the Milky Way, the M31 mass in Papovich is $\log M_* \sim 11$ at $z \sim 0$ and is thus just slightly lower mass than the systems recovered with our 3×10^{-4} Mpc^{-3} selection..

2.4 SFRs and dust extinction

The SFRs used in this work are derived using the rest-frame UV luminosity. A full explanation of this technique can be found in Ownsworth et al. (2014). We briefly explain the technique here. The rest-frame UV light traces the presence of young and short-lived stellar populations produced by recent star formation. The SFRs are calculated from scaling factors applied to the luminosities. These scaling factors are dependent on the assumed IMF (Kennicutt 1983). However, UV light is very susceptible to dust extinction and a careful dust correction has to be applied. The correction we use here is based on the rest-frame UV slope.

The raw 2800 Å NUV star formation rates ($\mathrm{SFR_{2800,SED}}$) used in this paper are obtained from the rest-frame near-UV luminosities measured from the best-fitting SED model found in the stellar mass fitting. We determine the dust-uncorrected SFRs, $\mathrm{SFR_{2800,SED,uncorr}}$, for $z = 0.5$–3 galaxies from applying the *Galaxy Evolution Explorer* NUV filter to the best-fitting individual galaxy SED.

To measure the SFR we first derive the UV luminosity of the galaxies in our sample, then use the Kennicutt (1998) conversion from 2800 Å luminosity to SFR assuming a Chabrier IMF:

$$\mathrm{SFR_{UV}(M_\odot\ yr^{-1})} = 8.24 \times 10^{-29} L_{2800}(\mathrm{erg\ s^{-1}\ Hz^{-1}}). \quad (2)$$

To obtain reliable SFRs in the rest-frame ultraviolet, we need to account for the obscuration due to dust along the line of sight. The way we do this is largely outlined in Meurer, Heckman & Calzetti (1999), who found a correlation between attenuation due to dust and the rest-frame UV slope, β, for a sample of local starburst galaxies, such that

$$f_\lambda \sim \lambda^\beta, \quad (3)$$

where f_λ is the flux density per wavelength interval and λ is the central rest wavelength. Using the 10 UV windows defined by Calzetti, Kinney & Storchi-Bergmann (1994) we measure β values from the best-fitting SED template for each galaxy. We can do this as the redshift range we are examining has well calibrated UV SED fits due to many of the input photometric bands lying in the UV part of the spectrum. These β values are then converted into a UV dust correction using the (Fischera & Dopita 2005, FD05) dust model. This dust calculation originates from the same method that we use to calculate the stellar masses, as a result our dust values are quantized into the units in which we apply the dust extinction to our model SEDs.

Whilst we show and discuss the A_{2800} dust extinctions in this paper, these can be converted using the relation between the extinction at other wavelengths. To ease comparison with other papers, the conversion of $A_V = 0.49 \times A_{2800}$ is applicable. More details of this method are discussed and presented in Ownsworth et al. (2014) for the sample we use throughout this paper.

2.5 Galaxy structural parameters

We calculate structural parameters measured on ground based UDS K-band images using GALAPAGOS (Galaxy Analysis over Large Area: Parameter Assessment by GALFITing Objects from SExtractor; Barden et al. 2012). This program uses SExtractor and GALFIT to fit Sérsic light profiles (Sérsic 1968) to objects in the UDS field. The Sérsic light profile is given by the following equation:

$$\Sigma(R) = \Sigma_e \times \exp\left(-b_n\left[\left(\frac{R}{R_e}\right)^{1/n} - 1\right]\right). \quad (4)$$

Where $\Sigma(R)$ is the surface brightness as a function of the radius, R; Σ_e is the surface brightness at the effective radius, R_e; n is the Sérsic index and b_n is a function dependent on the Sérsic index. The sizes (effective radius) are calibrated with galaxy sizes derived from the UDS area from the *Hubble Space Telescope* Cosmic Assembly Near-infrared Deep Extragalactic Legacy Survey (Grogin et al. 2011; Koekemoer et al. 2011) by van der Wel et al. (2012). For a full description of this method see Lani et al. (2013), where it is shown that the ground-based size measurements are reliable for galaxies with $K < 22$ in the UDS. Some of the galaxies at our highest redshifts are fainter than this, and we do not use those small fraction when calculating the structural parameters. We previously discussed these results and fits in Ownsworth et al. (2014) where we describe the size evolution of this sample.

As the redshift range which we probe is quite large, $1 < z < 3$, the rest-frame wavelength range we probe with the K-band varies significantly. This produces a morphological k-correction, whereby we are probing rest-frame J band at $z \sim 1$ and the rest-frame V band at $z \sim 3$. To address this we also measure the morphological parameters in shorter bands – J and H, and find essentially the same structural parameters. This is consistent with previous results which show that the structure and morphology is very similar for galaxies redward of the Balmer break for both nearby and distant galaxies (e.g. Taylor-Mager et al. 2007; Conselice et al. 2011).

2.6 Constant galaxy number density selection

We define our galaxy sample in the same way as in Ownsworth et al. (2014) using a constant galaxy number density selection at redshifts $z < 3$. In principle, selecting galaxies at a constant number density directly tracks the progenitors and descendants of massive galaxies at all redshifts. Studies such as Leja, van Dokkum & Franx (2013) and Mundy et al. (2015) have shown that this technique is robust at recovering the properties of the progenitors of local massive galaxies when using semi-analytic models. These models trace individual galaxies evolving over the last eleven billion years.

However, as shown in Mundy et al. (2015) when examining low and high-redshift galaxies the selected systems only have an overlap of at most 50 per cent. This means there is a 50 per cent contamination rate of galaxies that were not in the sample at high redshift but entered it at lower redshifts. However, the properties of the galaxies replacing initial members are very similar to those being replaced (see Section 3).

Table 1. Stellar mass function best-fitting Schechter function parameters from Mortlock et al (2015).

z	$\log(M_*)(M_\odot)$	$\log(\Phi^*)$	α
0.3–0.5	11.32 ± 0.07	-3.20 ± 0.08	-1.41 ± 0.02
0.5–1.0	11.16 ± 0.04	-3.12 ± 0.05	-1.34 ± 0.02
1.0–1.5	11.04 ± 0.04	-3.21 ± 0.06	-1.31 ± 0.03
1.5–2.0	11.15 ± 0.06	-3.74 ± 0.09	-1.51 ± 0.03
2.0–2.5	11.02 ± 0.10	-3.78 ± 0.14	-1.56 ± 0.06
2.5–3.0	11.04 ± 0.11	-4.03 ± 0.16	-1.69 ± 0.06

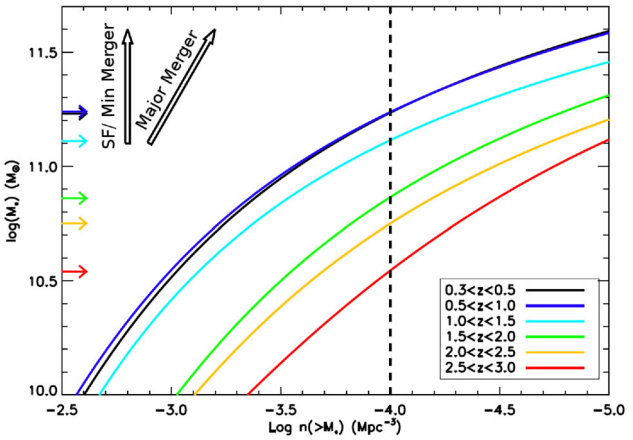

Figure 1. The integrated stellar mass functions from $z = 0.3$ to 3 from Mortlock et al. (2015). These integrated stellar mass functions gives us the comoving number density of all galaxies more massive than at a given stellar mass. The large open black arrows indicate the expected evolution due to star formation, minor mergers, and major mergers. We compare galaxies at a constant number density by selecting galaxies at each redshift at limits of $n(> M_*) = 10^{-4}$ Mpc^{-3}. The black dashed vertical line denotes the constant number density of 10^{-4} Mpc^{-3}. The coloured arrows indicate the values of M_* that correspond to this number density for each integrated stellar mass fraction.

In this study, we select and compare galaxies at three constant comoving number density values of $n = 3 \times 10^{-4}$, 10^{-4}, and 0.1×10^{-4} Mpc^{-3} at redshifts $0.3 < z < 3$ in six redshift bins. We chose these number densities as a trade-off between having a robust number of galaxies in the analysis at each redshift, and retaining a mass complete sample at the highest redshifts. This number density range is comparable to number densities used in other similar studies (e.g. Papovich et al. 2011, 2015; Conselice et al. 2013; Ownsworth et al. 2014).

We select our sample based on the integrated mass functions of the UDS field over the redshift range of $z = 0.3$–3.0 from Mortlock et al. (2015). The stellar mass profile fits as a function of redshift in which we use to calculate the relationship between number density and mass is shown in Table 1. Fig. 1 shows the integrated mass functions from Mortlock et al. (2015) and the lower stellar mass limits for the constant number density selection. The values for the limits are also listed in Table 2. The arrows in the top-left of Fig. 1 show how the galaxy stellar mass functions will change due to stellar mass growth through star formation and merging.

Table 2. Stellar mass limits for constant number densities used in this paper taken from the integrated mass functions shown in Fig. 1.

Redshift (z)	Stellar mass limit ($\log M_\odot$)		
	(3×10^{-4} Mpc^{-3})	(10^{-4} Mpc^{-3})	(10^{-5} Mpc^{-3})
0.3–0.5	10.95 ±0.05	11.24 ± 0.07	11.59 ±0.04
0.5–1.0	10.97 ±0.04	11.24 ± 0.04	11.58 ±0.04
1.0–1.5	10.84 ±0.05	11.11 ± 0.04	11.45 ±0.04
1.5–2.0	10.51 ±0.08	10.86 ± 0.05	11.31 ±0.05
2.0–2.5	10.40 ±0.09	10.75 ± 0.07	11.20 ±0.06
2.5–3.0	10.16 ±0.09	10.54 ± 0.09	11.11 ±0.04

3 RESULTS

Using our galaxy selection methods based on the different values of the comoving number density we examine the properties of galaxies selected through this method. That is, we examine the colour evolution, the passive galaxy fraction evolution, and the dust evolution between $z = 0.5$ and 3.

Before we discuss the properties of these galaxies, we give a brief background to the analysis here and how our results can be interpreted. First, Ownsworth et al. (2014) studied the evolution of the stellar mass and SFRs for galaxies selected with a variety of number densities. As our canonical comoving number density we use in this paper is $n = 10^{-4}$ Mpc^{-3}, we discuss briefly the results of Ownsworth et al. (2014) where the mass evolution of this sample is examined. Other number densities give slightly different results, however, as outlined in the appendix.

Using a number density selection of $n = 10^{-4}$ Mpc^{-3} we find that the mean stellar mass for this selection changes from $\log M_* = 10.6$ at $z \sim 3$ up to $\log M_* = 11.3$ at $z = 0$. Over this time period the mass of these galaxies grows by a factor of ∼4. This implies that of the total stellar mass in a $n = 10^{-4}$ Mpc^{-3} selected sample at $z = 0.5$, only 25 per cent of that mass would have been already within the galaxy at $z = 3$. We show that a significant fraction of the mass in these galaxies formed through other methods beyond star formation, with the most obvious possibility being merging. Ownsworth et al. (2014) furthermore discuss how the stellar mass built-up comes from equal amounts of merging and gas accretion. It is therefore now worth asking the follow-up question about the state of these galaxies as they evolve through this time.

In a similar study, Mundy et al. (2015) investigate the reliability of using a comoving volume sample to examine the evolution of galaxies. The goal in Mundy et al. (2015) was to determine the fraction of galaxies selected in a sample which remain in that sample at lower redshifts (purity) and the contamination of new galaxies when using a number density selection. Mundy et al. (2015) find that it is impossible to retrieve exactly the same galaxies through cosmic time, with purity and completeness levels at ∼50 per cent from $z = 3$ to 0. As described earlier, when using a stellar mass cut, such as $\log M_* = 11$ through all redshifts, the contamination fraction becomes as high as 95 per cent as early as $z \sim 1$ starting with a sample at $z \sim 3$ (Mundy et al. 2015).

However, Mundy et al. (2015) showed that while a galaxy sample selected at a constant number density selection can be contaminated, the properties of the galaxies replacing the galaxies removed are very similar to each other. Mundy et al. (2015) show that the average and integrated masses and SFRs chosen through a number density selection is very close to values of the initially selected sample, to within 50 per cent, and often much lower (Mundy et al. 2015). This shows that while the samples are not the same through time, the properties inferred are similar to what would be measured if the identical samples could be retrieved completely. We therefore adopt this approach of using number density selection for understanding the evolution of a galaxy population, with these caveats and assumptions spelled out.

3.1 Colour evolution

3.1.1 Method

The first thing we examine within our constant comoving number density selection is the stellar populations of the galaxies selected through this methodology.

We do this in several ways, but the initial methodology for investigating these galaxy's is through their position in the *UVJ* digram. The rest-frame $U - V$ versus $V - J$ diagram is a useful tool to separate quiescent and star-forming galaxies. It has become commonly used due to its ability to distinguish between truly quiescent objects and dust reddened systems at redshifts $z \sim 2$ (e.g. Williams et al. 2009). Many alternative methods exist to separate a galaxy population into star-forming and passive objects using broad-band photometry e.g. *g–r* colour (Bell et al. 2003), *u–r* colour (Baldry et al. 2004), *U–B* colour (Peng et al. 2010) and *BzK* colours (Daddi et al. 2004) see Taylor et al. (2015) for a comparison of these techniques. We use the *UVJ* method as it is has been used extensively at high redshifts and is therefore the best understood in principle (e.g. Mortlock et al. 2015). More details in how we use the *UVJ* diagram and its limitations is described for our sample in Mortlock et al. (2015) and a further test is done in this paper in Section 3.2.

The selection we use is based on the *U*, *V*, and *J* Bessel band rest-frame luminosities. These were also used by Williams et al. (2009) to select evolved stellar populations from those with recent star formation at $z < 2$. This technique is also used in Hartley et al. (2013) to extend the passive galaxy selection out to higher redshifts. The selection criteria for passive galaxies are as follows:

$$U - V > 0.88 \times V - J + 0.69 (z < 0.5) \quad (5)$$

$$U - V > 0.88 \times V - J + 0.59 (0.5 < z < 1.0) \quad (6)$$

$$U - V > 0.88 \times V - J + 0.49 (z > 1.0) \quad (7)$$

with $U - V > 1.3$ and $V - J < 1.6$ in all cases. Although these criteria efficiently select galaxies with old stellar populations, there is a possibility that the 'red' sample could still be contaminated by dusty star-forming galaxies, edge on discs or AGN. We minimize this contamination by using the wealth of multiwavelength data that is available in the UDS field.

To identify active galaxies we cross-match our sample with surveys taken at X-ray and radio wavelengths. For the X-ray we use data from the Subaru/*XMM–Newton* Deep Survey (Ueda et al. 2008) which covers the UDS field over the energy range of 0.5–10 keV. For the radio, we use data from Simpson et al. (2006) which utilizes VLA 1.4 GHz data. We remove any galaxies that have either a detection in the X-ray or radio to clean this sample of AGN. This data will only effectively select out AGN at $z \lesssim 1$ due to the limits of these surveys, and will only be able to select the most radio loud and very active AGN at higher redshifts.

Furthermore the 24 μm data from the SpUDS provides a way to identify red objects that harbour dust-enshrouded star formation. Therefore any objects with a 24 μm detection (> 300 μJy, 15σ) are assumed to be dusty star-forming objects. Any galaxy found to be passive via the *UVJ* selection criteria, but which has a bright 24 μm source associated with it will be reassigned to the star-forming population and have a full UV dust correction applied. We are

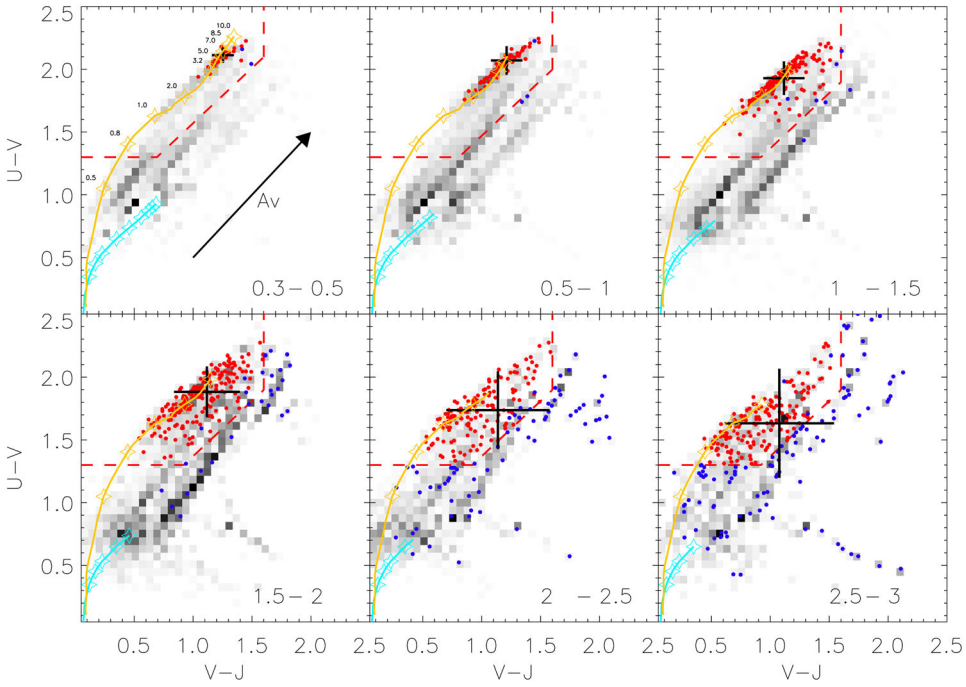

Figure 2. Rest-frame $U-V$ versus $V-J$ diagram in redshift bins between $z=0.3$ and 3.0 of the constant number density selected sample with $n = 10^{-4}$ Mpc^{-3}. This corresponding to a mass limit of log $M_* \sim 11.24$ at $z \sim 0.3$. The red dashed lines denotes the *UVJ* passive selection. Red circles show the progenitors of massive galaxies that are selected as passive via the *UVJ* method. Blue circles show the progenitors of massive galaxies that are selected as star forming via the *UVJ* method and 24 μm criteria. The black cross shows the median colour and standard deviation for the progenitor sample in each redshift bin. Grey-scale shows total population selected above the 95 per cent completeness limit within each redshift bin. The colour evolution tracks from Bruzual & Charlot (2003) SSP models are also shown. The light blue line shows a constant star formation history with no dust and the yellow line shows an exponentially declining star formation history with $\tau = 0.1$ Gyr. The blue open stars represent model colours at the specified ages, given in Gyr. These have the same intervals as the orange line and are at: 0.5, 0.8, 1.0, 2.0, 3.5, 5.0, 7.0, 8.5, 10.0 Gyr. The colour evolution tracks are plotted up to the age of the Universe in each redshift bin. Similar plots at other number densities can be found in the appendix.

careful to exclude those objects that have an AGN signature, either through X-ray emission or through signatures in those that have spectra. In total ∼2 per cent of objects selected as being passive via the *UVJ* criteria were reassigned to the star-forming sample through this method.

3.1.2 *Stellar population ages*

Fig. 2 shows the *UVJ* diagram for the constant number density sample with $n = 10^{-4}$ Mpc^{-3} in different redshift bins. The red box region plotted in Fig. 2 is from Williams et al. (2009) and denotes the passive galaxy selection. Red points show galaxies that are selected as passive and blue points show galaxies that are selected as star forming within the given redshift bin. The large cross in each redshift plot denotes the median value for the whole progenitor population within each redshift bin. The grey-scale shows the total population selected above the 95 per cent stellar mass completeness limit for the UDS sample from Hartley et al. (2013).

Our *UVJ* diagram in Fig. 2 is similar to previous work (e.g. Williams et al. 2009; Brammer et al. 2011; Marchesini et al. 2014; Papovich et al. 2015) with some exceptions. These previous studies in general are examining galaxies which contain a larger range, and thus lower, stellar masses than we examine in this paper. If one restricts these previous diagrams to a high stellar mass limit, then one finds a good overlap as in Papovich et al. (2015) for the M31 progenitors, which are less massive than our nominal $n = 10^{-4}$ Mpc^{-3} selected sample, but more similar to our $n = 3 \times 10^{-4}$ Mpc^{-3} limit. Furthermore, we only use this diagnostic to determine the difference between star-forming and passive populations.

Although we do not discuss these results in this paper, our *UVJ* colour selection clearly correlates with galaxy morphology (passive=elliptical, star forming = disc+peculiar) (Margalef-Bentabol et al. 2016) as well as with galaxy clustering, whereby the passive galaxies are clearly more clustered than the blue systems (e.g. Hartley et al. 2013; Wilkinson et al. 2016). Thus this method does well in separating blue star formation from red passive systems.

As can be seen from Fig. 2, within the lowest redshift bin ($z=0.3$–0.5) the massive galaxy population constitutes a homogeneous population with extremely red $U-V$ colours with very little scatter. Moving to higher redshifts the scatter increases, and the population becomes more diverse in both $U-V$ and $V-J$ colours. However, as this population diversifies towards higher redshifts we find that the median *UVJ* colour remains at all redshifts within the passive region, albeit with a larger scatter. When we compare similar mass ranges to those of Papovich et al. (2015), which are presented in the appendix, we find a similar average colour evolution, to within or better than 0.3–0.5 dex, in $(U-V)$ and $(V-J)$ colours, a difference which is within the uncertainties. However, Marchesini et al. (2014) find a significantly different pattern for the evolution of massive galaxies from this paper and Papovich et al. (2015).

Also in Fig. 2, we have plotted evolutionary tracks for the two colours from Bruzual & Charlot (2003) single stellar population models. The light blue line is a constant star formation history with no dust, and the yellow line is an exponentially declining star formation history with $\tau = 0.1$ Gyr and zero dust attenuation

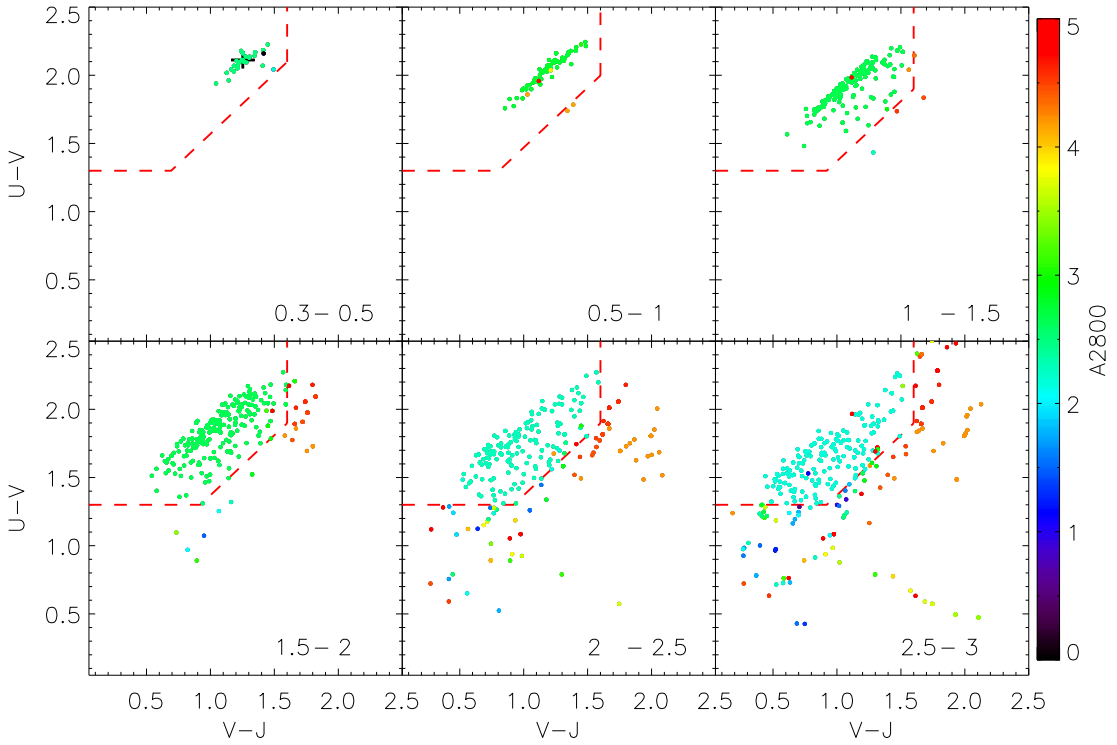

Figure 3. Similar to Fig. 2, but showing the dust content of each galaxy. Rest-frame $U - V$ versus $V - J$ diagram in redshift bins between $z = 0.3$ and 3.0 of the constant number density selected sample with $n = 10^{-4}$ Mpc^{-3}. Coloured circles show the progenitors of massive galaxies with the colour representing the UV dust attenuation at 2800 Å as shown by the colour bar on the right-hand side.

starting at the different labelled look back times. Comparing with these models we find that at $z < 0.5$ the progenitors of local massive galaxies harbour old (ages older than 5 Gyr) stellar populations which can be explained by an exponentially declining star formation history.

Examining the progenitors at higher redshifts, the median *UVJ* colours within the error is always consistent with the exponentially declining models, showing that a large fraction of this population is passively evolving. If we consider the effect of dust, the average age of the stellar populations for these galaxies would decrease with increasing dust attenuation. As we move to higher redshift both the constant star formation evolution track with zero dust, and the exponentially declining star formation history without dust does not accurately trace the whole star-forming population, therefore this clearly indicates that the star-forming progenitors must contain significant amounts of dust.

In the appendix we show the analog *UVJ* diagrams for other number density selections, namely: $n = 0.1 \times 10^{-4}$ and $n = 3 \times 10^{-4}$ Mpc^{-3}. Both of these number density selections show similar behaviour as the $n = 10^{-4}$ Mpc^{-3} selected sample. In the lowest redshift bin the galaxy population at all number density selections are a homogeneous population with red $U - V$ colours, with a small amount of scatter. Examining the $n = 3 \times 10^{-4}$ and $n = 0.1 \times 10^{-4}$ Mpc^{-3} populations towards higher redshifts we find a similar result as the $n = 10^{-4}$ Mpc^{-3} galaxy population. The median *UVJ* colour remains at all redshifts within the passive region.

3.1.3 *Dust extinction*

In Fig. 3, we examine the dust extinction properties of the progenitor galaxy sample. In Fig. 3, the progenitor galaxies are colour coded to represent their dust extinction at 2800 Å (A2800) measured from the UV slope. The uniformity of the passive objects in Fig. 3 arises from the method we used to derive the dust correction for these objects (e.g. see Ownsworth et al. 2014). Of the objects that are selected as star-forming systems we find that at $z > 1.5$ there is a diverse population of objects from dust-poor objects lying towards the bottom left-hand corner to highly dust attenuated systems lying towards the top right-hand corner as expected for the *UVJ* colour selection. The total star-forming population at $z > 1.5$ has an average 2800 Å dust correction of ∼3.7 mag.

We find a significant evolution in dust content over the redshift range $1.5 < z < 3.0$ for dust-poor objects, those with a low $V - J$ colour. These dust-poor objects are quite abundant at $z \sim 2.5$, with 28 ± 4 per cent of star-forming galaxies with $V - J < 1.0$, and decreasing towards $z = 1.5$, where only 6 ± 2 per cent of star-forming galaxies have $V - J < 1.0$. We also find that a small population, 10 ± 4 per cent, of the star-forming progenitors show rest-frame $U - V$ colours redder than, or as red as, the quiescent progenitors.

At higher redshifts, $z > 2.5$, these objects span a wide range of rest-frame colour values. Examining the derived UV-slopes for the star-forming population we find that the fraction of highly attenuated systems increases with higher redshift, similar to the result before. We find that 5 ± 3 per cent of the star-forming population at $z = 3$ have $A_{2800} > 5$ mag, increasing to 14 ± 4 per cent at $z = 1.5$. This is accompanied by a decrease in the low dust attenuated systems, with 12 ± 3 per cent of the star-forming population with $A_{2800} < 2$ mag at $z = 3$, decreasing to 2 ± 2 per cent at $z \sim 1.5$. This suggests that the star-forming progenitors at this redshift contain a wide range of dust and star formation properties unlike their low-redshift descendants (see also Whitaker et al. 2012; Kaviraj et al. 2013). We explore this

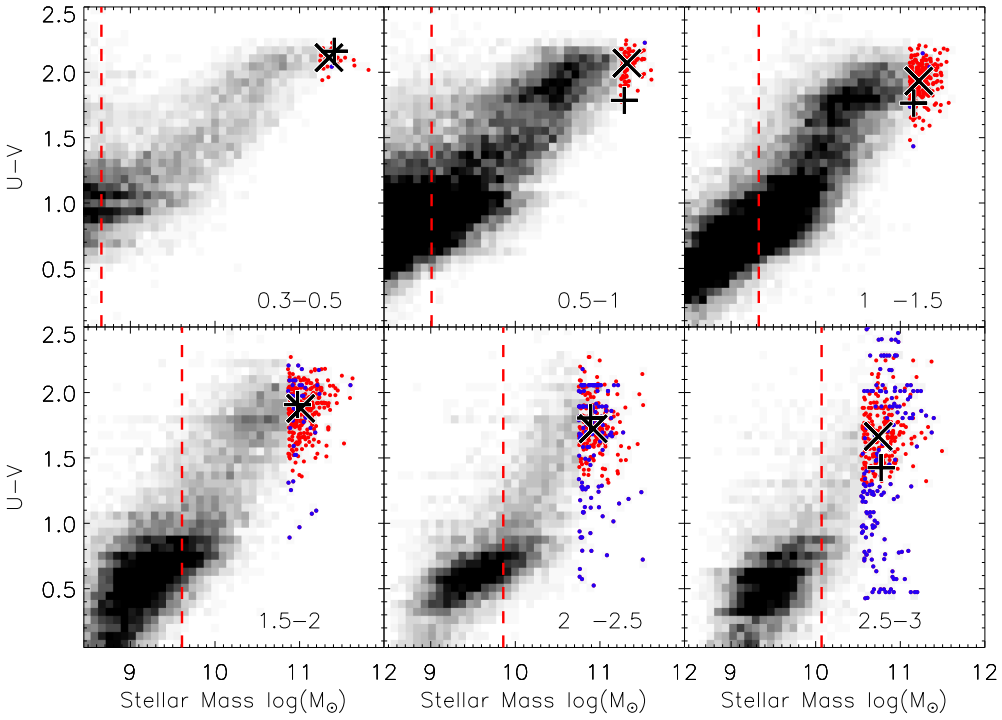

Figure 4. Stellar mass versus rest-frame $U - V$ colour for all galaxies selected via the constant number density selected sample with $n = 1 \times 10^{-4}$ Mpc^{-3}. The red circles show the progenitors of massive galaxies that are selected as passive via the *UVJ* method. The blue circles show the progenitors of massive galaxies that are selected as star forming via the *UVJ* method. The black 'X' shows the median $U - V$ colour for the passive population and the black plus '+' sign shows the median $U - V$ colour for the star-forming population. The grey-scale shows the whole UDS galaxy sample within each redshift bin. The red dashed line shows the 95 per cent stellar mass completeness limit.

in more detail in relation to the stellar mass of these systems later in this paper.

3.2 Evolution in colour versus stellar mass

As highlighted in the previous section, the progenitors of local massive galaxies at relatively low redshift ($z < 1$) have similar colours, typical of quiescent and old stellar populations. As we look towards higher redshifts, some progenitors at our constant number density of $n = 10^{-4}$ Mpc^{-3} become star forming (Section 3.1). We find that some of the star-forming progenitors exhibit a wide range of $U - V$ colours. We examine this result in a different way in Fig. 4 using the $U - V$ rest-frame colour versus stellar mass. Fig. 4 shows the star-forming and quiescent samples selected in the same way as in Fig. 2. The red dashed line shows the 95 per cent stellar mass completeness limit within each redshift interval. The blue points show the star-forming progenitors with the median of this population represented by the black plus symbol '+'. The red points show the quiescent progenitors with the median of this population represented by the black cross, 'X'. The grey-scale show the total galaxy population within each redshift interval.

We find that at the lowest redshift, the massive galaxy progenitors have very small scatter in both colour (∼0.08 mag) and stellar mass, with the scatter increasing at higher redshifts. In fact at this epoch the mean colour and stellar mass for the blue and red systems is statistically identical, although there are very few blue systems to compare with at the lower redshifts.

Examining this trend at higher redshifts the median for both the star-forming and passive population do not show a large evolution, with the median $U - V$ colour of the star-forming progenitors becoming bluer by 0.7 ± 0.6 mag over $0.3 < z < 3$, and the median colour for the passive progenitors becoming bluer by 0.5 ± 0.2 mag over the same epoch. Fig. 4 demonstrates that the average star-forming progenitor has a similar optical colour as a passive progenitor at the same redshift. Fig. 4 also shows that the average star-forming progenitor has not lived in the blue star-forming cloud since at least $z = 3.0$, although there are a significant number that do.

However, upon examining the population of star-forming progenitors in more detail we find that 27 per cent at $z = 3.0$ have blue, $U - V < 1.0$, colours comparable to galaxies living on the $z = 3.0$ blue cloud. Conversely, 24 per cent of the star-forming progenitors at $z = 3.0$ also have extreme red, $U - V > 2.0$, colours. Examining the galaxies in our selection at $z = 3.0$ that have red $(U - V)$ colours we find that the star-forming systems are more numerous than the passive *UVJ* selected progenitors by a ratio of 3 : 1. The larger scatter in $U - V$ colours of the star-forming progenitors is more pronounced than in the passive progenitors, i.e. 0.6 mag for star forming and 0.2 mag for passive at $z = 3.0$. The evolution in scatter between low and high redshift shows that the local red sequence is in the process of assembly between $0.3 < z < 3.0$.

In the appendix, we show the $U - V$ rest-frame colour versus stellar mass of the $n = 10^{-5}$ and $n = 3 \times 10^{-4}$ Mpc^{-3} selections. We find that the lower number density galaxy sample of $n = 10^{-5}$ Mpc^{-3} has a very small scatter (∼0.2 mag) in $U - V$ colours across the whole redshift range studied. This suggests that these very high mass galaxies have undergone the majority of their colour evolution at $z > 3$ (e.g. Duncan et al. 2014). The higher number density galaxy sample of $n = 3 \times 10^{-4}$ Mpc^{-3}, sampling

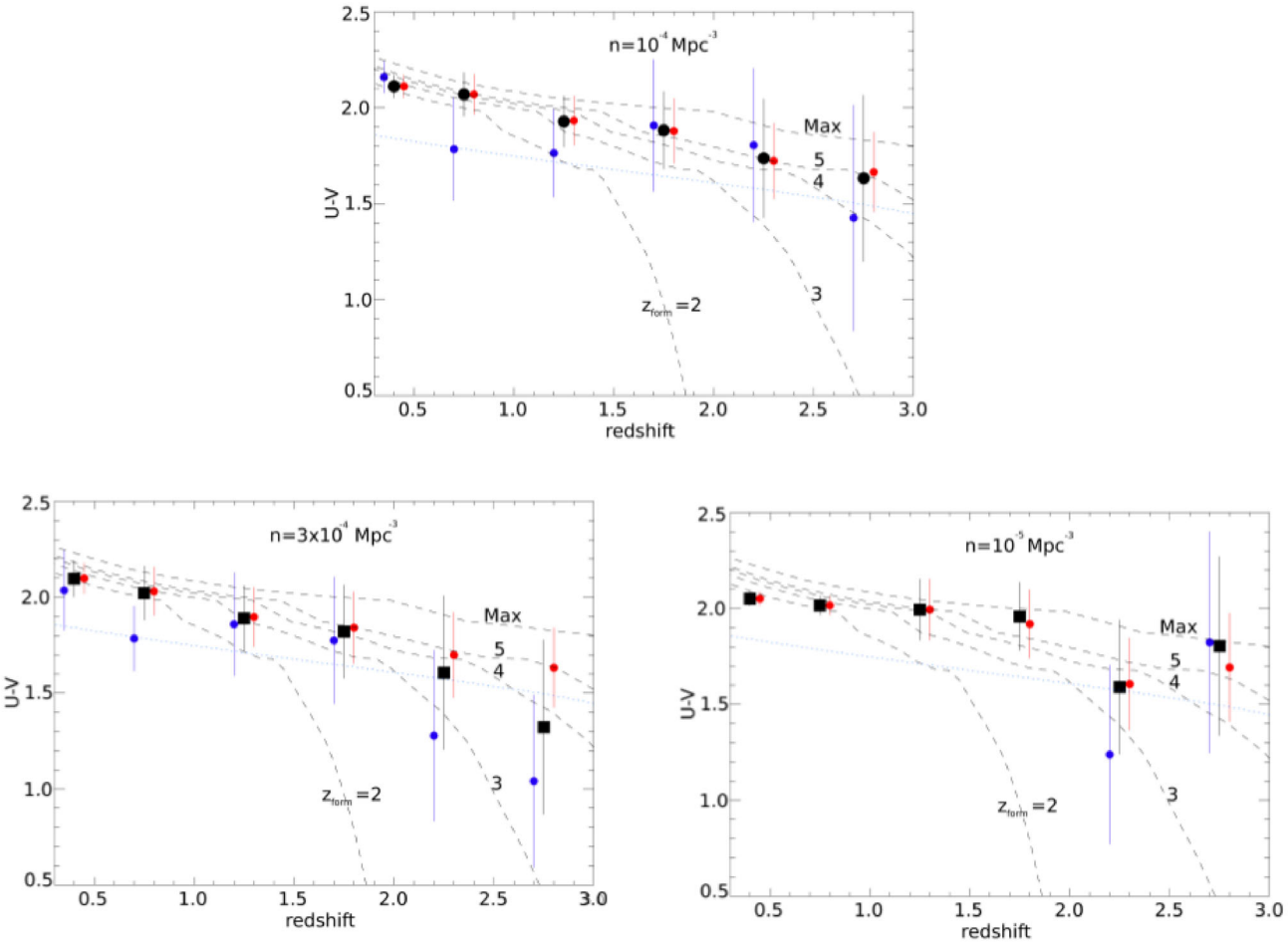

Figure 5. Median rest-frame $U - V$ colour versus redshift for constant number density selected samples at three different number densities. The black circles and squares show the evolution of the median $U - V$ colour of the whole progenitor population. The red and the blue circles show the evolution of the median $U - V$ colour of the passive and star-forming samples, respectively. Also shown is the colour evolution tracks from Bruzual & Charlot (2003) models for a exponentially declining star formation history starting at the labelled redshift. The black dashed lines show the colour evolution of a declining star formation history and varying formation redshifts starting from the beginning of the Universe (Max) to $Z_{\rm form} = 2$. The light blue dotted line shows the colour evolution of a constant star formation history and $A_{\rm v} = 2$ mag of dust extinction. This level of dust extinction is equivalent to the average dust correction of the star-forming progenitors.

typically lower mass galaxies, shows an increasingly large scatter towards higher redshifts with 31 per cent of the progenitors of local $n = 3 \times 10^{-4}\,{\rm Mpc}^{-3}$ galaxies lying on the blue cloud with blue, $U - V < 1.0$, colours. Compared to the $n = 10^{-4}\,{\rm Mpc}^{-3}$ galaxy population the star-forming progenitors of the $n = 3 \times 10^{-4}\,{\rm Mpc}^{-3}$ galaxy population transition on to the red sequence at lower redshifts. This in an indication of galaxy 'downsizing' which can be seen within galaxy selection based on number density in addition to stellar mass.

In Fig. 5 we show how the median $U - V$ colours for the total (black squares), star forming (blue circles) and, passive (red circles) evolve with redshift. Also plotted are the $U - V$ colour evolution tracks derived from Bruzual & Charlot (2003) SSP models with an exponentially declining star formation history as shown in Fig. 2 plotted as the black dashed lines, and one with a constant star formation history with $A_{\rm v} = 2$ mag of dust extinction, comparable to the average dust correction of the star-forming population, shown by the light blue dotted line in Fig. 2.

These model tracks have a varying formation redshift from the beginning of the Universe (Max) down to $Z_{\rm form} = 2$. The total population progenitors show a gradual evolution in their $U - V$ colours towards redder colours at lower redshifts, indicative of an aging stellar population that formed at redshifts of $z > 4$. Dividing the population into star forming and passive we find that the passive population follows the passively evolving colour tracks with hints that they may have stopped actively forming stars at redshifts as high as $z = 5$.

We also examine the effects of increased dust extinction on these age derivations. The overall effect of dust is to decrease the formation redshift. The average colours at low redshift are consistent with some dust extinction, around $A_{\rm NUV} = 1.5$, as we found through our fits to the SEDs of these galaxies. When examining higher redshifts, where there is more parameter space available for different scenarios, we find that the colours are consistent with a $z_{\rm form} = 5$, but with no dust extinction. As we do find some dust absorption through the SED fits, then a more realistic scenario also consistent with our colours is a formation redshift of $z_{\rm form} = 4$, with an extinction of $A_{\rm NUV} = 1$, or a formation redshift of $z_{\rm form} = 3$ with an extinction of $A_{\rm NUV} = 2$. Therefore these systems have a formation redshift of $z_{\rm form} > 3$.

The other number densities shown in Fig. 5 show a similar pattern, but with the lower number densities at $n = 10^{-5}$ Mpc^{-3} having a higher formation redshift than the 10^{-4} Mpc^{-3} selected systems, whilst the density selection of $n = 3 \times 10^{-4}$ Mpc^{-3} has a lower redshift of formation than the 10^{-4} Mpc^{-3} selection. This is another indication of the downsizing, but seen here through number density selections as opposed to stellar mass.

While the star-forming population appears to be following the declining star formation history colour evolution tracks, they are also consistent with the dust reddened constant star formation history colour evolution track. However, from Fig. 2 we see that they are not consistent with the exponentially declining star formation history when examined in combination with other colours.

This result shows that a population selected at a constant number density has formed the majority of its $z = 3$ stellar mass on average within the first Gyr of cosmic time. Is this plausible given our knowledge of the global cosmic star formation history? If we assume these objects formed their $z = 3$ stellar masses over the redshift range $5 < z < 9$ (∼0.6 Gyr) via star formation, the average SFR this implies is 114 M$_\odot$ yr^{-1}. Incorporating the number density of the progenitor galaxies, $n = 10^{-4}$ Mpc^{-3}, gives an SFR density of these objects of $\rho_{\rm SFR,progenitors} = 0.01$ M$_\odot$ yr^{-1} Mpc^{-3}. From various works (e.g. McLure et al. 2013; Duncan et al. 2014), the global cosmic SFR density over the redshift range $5 < z < 9$ varies from $\rho_{\rm SFR,cosmic} = 0.05 \pm 0.03$ M$_\odot$ yr^{-1} Mpc^{-3} at $z = 5$ to $\rho_{\rm SFR,cosmic} = 0.02 \pm 0.06$ M$_\odot$ yr^{-1} Mpc^{-3} at $z = 9$. As the global cosmic SFR density is larger than the SFR density inferred for the progenitor galaxies, it is therefore possible for these objects to form via star formation within the first Gyr of cosmic time.

3.3 Star formation history

Using our knowledge from the previous sections, we now examine how and when the progenitors of local massive galaxies became the quiescent objects we see today. In this section we examine the $n = 10^{-4}$ Mpc^{-3} number density sample.

Fig. 6 shows how the average specific star formation rate (sSFR = SFR/M_*) of the total, star-forming and, passive progenitor galaxies evolved from $z = 3.0$ for our sample using the number density selection $n = 10^{-4}$ Mpc^{-3}. The blue circles show the median sSFR of the *UVJ* selected star-forming progenitor galaxies, the red circles show the median sSFR of the *UVJ* selected passive progenitor galaxies and the black squares show how the median sSFR of the whole population evolves across this redshift range. For the higher and lower number densities discussed in the appendix, we find essentially the same pattern. Also shown in Fig. 6 are lines denoting different stellar mass doubling times, i.e. the time it to takes for ongoing SFR to double the stellar mass of a given galaxy. The dot–dashed line denotes a doubling time equal to the age of the Universe at $z = 0$, a passivity selection made in the local Universe. The dashed line shows a doubling time equal to the age of the Universe at a given redshift. Note that this doubling time at a given redshift appears to be a good dividing line between *UVJ* passive and star-forming systems.

Not surprisingly, we find that the evolution of the sSFRs of the passive progenitor galaxies is faster than for star-forming systems. The passive progenitor galaxies' median sSFR decreases with redshift by 1.5 ± 0.3 dex from $z = 3.0$. The star-forming progenitor galaxies median sSFR also decreases over the same time interval by only 0.8 ± 0.4 dex. If we examine the divide between the two

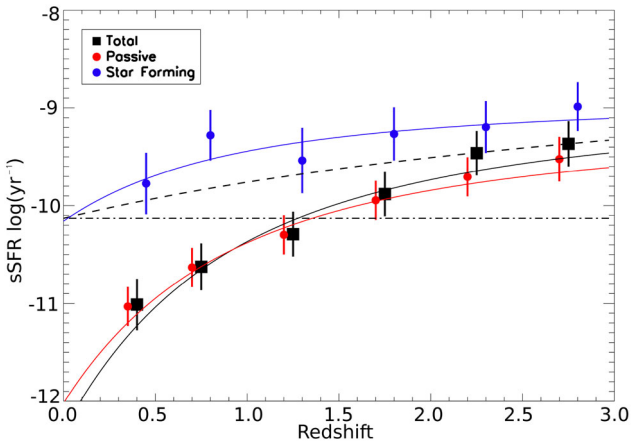

Figure 6. The average sSFR versus redshift for all galaxies selected via the constant number density selected sample with $n = 10^{-4}$ Mpc^{-3}. Black squares show the evolution of the whole population. Red circles show galaxies that are selected as passive via the *UVJ* method. Blue circles show galaxies that are selected as star forming via the *UVJ* method. The horizontal dot–dashed line represents a stellar mass doubling time equal to the age of the universe at $z = 0$. The dashed line represents a stellar mass doubling time equal to the age of the universe at a given redshift. The solid red, blue, and black lines show the best-fitting exponentially declining star formation histories for the passive, star-forming, and total progenitor population, respectively (see text). The errors of the fractions are derived from Monte Carlo analyses.

populations, at low redshifts the difference in sSFR is more pronounced than at higher redshifts, with ΔsSFR $= 1.2 \pm 0.2$ dex at $z = 0.3$ and ΔsSFR $= 0.5 \pm 0.4$ dex at $z = 3.0$. We quantify the sSFR histories of the progenitor galaxies by fitting an exponentially declining model of the form

$$\mathrm{sSFR}(t) = \mathrm{sSFR}_0 \times \exp(-\mathrm{t}/\tau) \quad (8)$$

with $\tau = 1.9 \pm 0.8$ Gyr for the total progenitor galaxy population, $\tau = 2.1 \pm 0.4$ Gyr for the passive objects and $\tau = 4.7 \pm 0.5$ Gyr for the star-forming objects. The larger value of τ for the star-forming sample, compared to the passive objects, is as expected for a star-forming population (Ownsworth et al. 2014).

Using our knowledge of the sSFRs of the progenitor galaxies, in Fig. 7 we examine the validity of the *UVJ* colour selection. Fig. 7 shows the normalized histograms of the passive and star-forming populations as defined via the *UVJ* colour selections across the redshift range we study. We find that both populations appear to be single peaked distributions across the redshift range, with an increasing overlap towards higher redshifts. Therefore, the *UVJ* colour selection appears to be an effective measure in separating the two populations for these massive galaxies at the redshift ranges we study. We find a similar result for the other number densities we consider in the appendix.

We also examine the evolution of the SFR density of these progenitors of massive galaxies. Fig. 8 shows the evolution of the SFR density with redshift. The black squares show the evolution of the total progenitor population and the red and blue circles show the passive and star-forming objects, respectively. Also shown in Fig. 8 is the global SFR history (SFH) from Hopkins & Beacom (2006) using the form from Cole et al. (2001), $\rho(t) = (a + bz)h/(1 + (z/c)^d)$ with $a = 0.017$, $b = 0.13$, $c = 3.3$, $d = 5.3$. The solid black line shows the best fit to the total progenitor population with the same

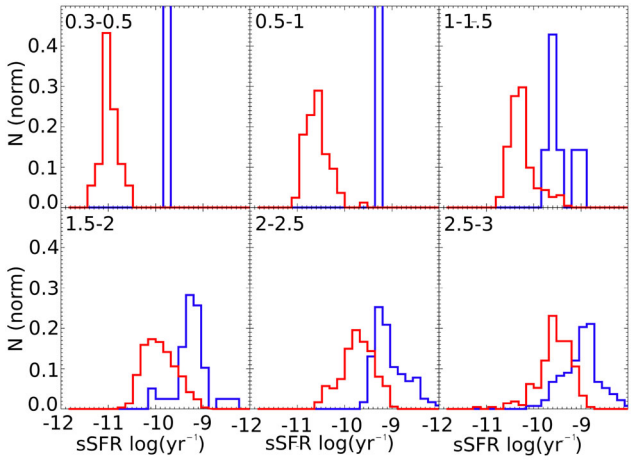

Figure 7. Histograms of the sSFRs of the *UVJ* defined passive and star-forming progenitor galaxies over the redshift range $0.3 < z < 3.0$ split into six redshift bins, which are labelled. The red histogram shows the sSFRs of the progenitors of local massive galaxies that are defined as passive via *UVJ* colour selection and blue shows those that are classified as star forming. Both the passive and star-forming histograms are normalized to the number of objects in each selection.

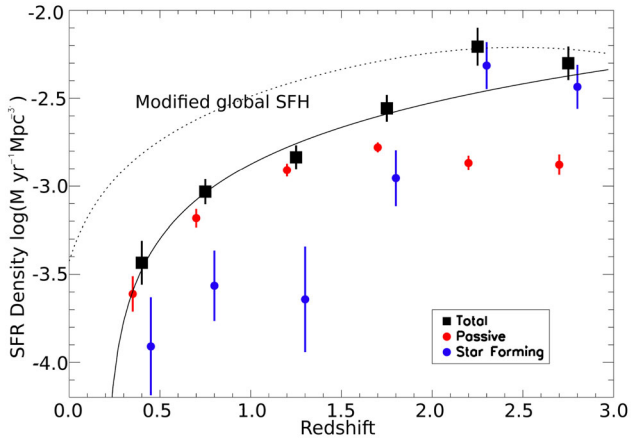

Figure 8. Star formation density versus redshift for all galaxies selected via the constant number density selected sample with $n = 10^{-4}$ Mpc^{-3}. The black squares show the evolution of the whole galaxy sample and the red and blue circles show the evolution of the star formation density of the passive and star-forming populations selected through *UVJ* colours. The errors on the densities are derived from Monte Carlo analysis. The dotted line shows the global star formation history from Hopkins & Beacom (2006) modified by −1.5 dex for clarity. The solid black line represents the best fit to the star formation density evolution of the total progenitor galaxy population.

form as the global SFH. We do not fit the SFR density evolution of the passive and star-forming populations as their evolution is driven by their individual abundances as well as their star formation history. Therefore, the evolution of the passive and star-forming SFR densities will not trace the same objects at all redshifts. We find that the progenitors of local massive galaxies appear to undergo a sharper decrease in their SFR density than the global galaxy population SFH. They also show evidence that their SFH peaks at a higher redshift than the global galaxy population SFH. Both of these findings are evidence for the downsizing scenario of galaxy formation.

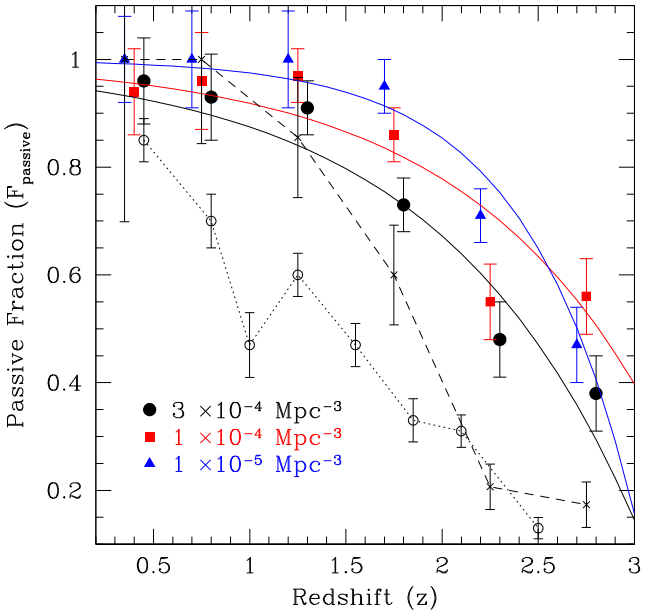

Figure 9. Passive, or quiescent, fraction of the number density selected samples selected at three different number densities: $n = 10^{-4}$ Mpc^{-3} (red boxes), $n = 10^{-5}$ Mpc^{-3} (blue triangles) and $n = 3 \times 10^{-4}$ Mpc^{-3} (black solid circles) versus redshift. The points at each number density selection denote the fraction of galaxies selected as passive via the *UVJ* method. The solid lines show the best fit to the passive fractions with the form of equation (9) at the three number densities with the colour of this line corresponding to the number density. The errors on our fractions are derived from Monte Carlo analysis. The dotted line at the bottom with open circle points is the passive fraction found by Papovich et al. (2015) for M31 mass galaxies, and the dashed line with the crosses for points shows the passive evolution for galaxies selected with abundance matching at masses log $M_* > 10^{11.8}$ by Marchesini et al. (2014).

3.4 Passive fraction evolution

We examine in this section the passive fraction for our canonical $n = 10^{-4}$ Mpc^{-3} selection, as well as the higher and lower density selections. We do this by using the information in the previous subsections including sSFRs, and the passivity versus star formation nature derived from the *UVJ* colour selection. In Fig. 9, we show evolution of the *UVJ* defined passive fraction of the progenitors of local massive galaxies. The red boxes show the fraction of galaxies that are selected as passive via this work. The red line is the best fit to the fraction with the form

$$F_{\rm passive} = 1 - (0.05 \pm 0.02) \times {\rm e}^{(1.0 \pm 0.2) \times z}. \quad (9)$$

We find that the passive fraction of progenitor galaxies for this selection undergoes a significant evolution over the redshift range $0.3 < z < 3.0$. Within our lowest redshift bin at $z \sim 0.5$, 94 ± 8 per cent of the progenitor galaxies are passive, much like their local universe counterparts. In our highest redshift bin ∼50 per cent of the progenitor galaxies are passive by $z \sim 2.5$. This implies that about half of the progenitors of today's massive galaxies had already stopped actively star forming by $z = 3.0$.

We find a similar trend for the other number densities used in this study, $n = 10^{-5}$ and $n = 3 \times 10^{-4}$ Mpc^{-3}, where we also find that the passive fraction is near 90 per cent by $z = 1.5$. In fact there does not appear to be a strong dependence on stellar mass, or number density selection, in how the fraction of galaxies which are passive evolve with time. This result however could easily reside in the uncertainties which arise from determining passive fractions.

However, there is a trend such that on average the higher mass and lower number density selected objects have a higher passive fraction at all redshifts.

This indicates that the average progenitor of local massive galaxies have had a red rest-frame colour since $z = 3$, although with a large scatter and with some blue galaxies. This is similar to, but slightly different, to the findings of Marchesini et al. (2014), who find that the progenitors of the local ultramassive galaxies (with $\log(M_*/\mathrm{M}_\odot) = 11.8$) have blue average rest-frame colours and ∼17 per cent are selected as passive at $z > 2.5$ (Fig. 9). Papovich et al. (2015) find an even lower fraction which is passive. Our result is higher in passive fraction likely due to the fact that our galaxies are more massive and thus more likely to be passive up to $z \sim 3$. However, this does not explain the tension with Marchesini et al. (2014) and there thus remains an unexplained inconsistency between our results and theirs.

The observed weakening of the colour–density relation at $z > 2$ (e.g. Chuter et al. 2011; Grützbauch et al. 2011) implies that the environments of galaxies have not been fully established at high redshift. Therefore, the role of environmental quenching mechanisms, such as ram pressure stripping, are unlikely to play a dominant role in the quenching of the progenitors of local massive galaxies at early cosmic times. The result that we present here shows that a large fraction of galaxies are already passive by $z = 3.0$ and implies that internal quenching mechanisms, such as the hot halo model, are likely responsible.

3.5 Sérsic index and size evolution

The present-day massive galaxy population is dominated by objects with early-type morphologies and high Sérsic indices (e.g. Baldry et al. 2004; Conselice 2006b; Buitrago et al. 2013). Examining similar stellar mass objects at $z > 2$ studies have found this not to be the case (e.g. Buitrago et al. 2013; Mortlock et al. 2013; Bruce et al. 2014). However, this has not been examined using a number density selected sample. Avoiding the precursor bias is critical, as when we compare a stellar mass selected sample we are obtaining samples which can be 95 per cent or more different between $z = 3$ and 0 (e.g. Mundy et al. 2015).

In Fig. 10(a) we show the evolution of the Sérsic indices of the progenitors of local massive galaxies at our measured density of $n = 10^{-4}$ Mpc^{-3}. The progenitor galaxies have been split into high and low Sérsic index systems with a dividing line at $n = 2.5$. The value of $n = 2.5$ has been used in many studies as a quantitative way to segregate between early- and late-type galaxies, with early-type galaxies having $n > 2.5$, although for mass-selected samples (e.g. Shen et al. 2003; Barden et al. 2005; McIntosh et al. 2005; Buitrago et al. 2013). The fraction of progenitors with high Sérsic indices is represented by the green rectangles, and the fraction with low Sérsic indices is represented by the black circles. Fig. 10(a) clearly indicates that the fraction of the progenitors of local massive galaxies with lower Sérsic indices has greatly increased with redshift, with 8 ± 5 per cent of the progenitor galaxies at $z = 0.3$ having low Sérsic indices, increasing to 65 ± 7 per cent at $z = 3$. We find essentially the same results at the other two number densities considered in the appendix.

If we take the assumption that objects with low Sérsic indices have a disc-like morphology, this result implies that the progenitor galaxies at high redshift are mostly discy galaxies. However, this assumption breaks down if we consider the effect of galaxies with disturbed and irregular morphologies. Both Buitrago et al. (2013) and Mortlock et al. (2013) showed that galaxies at high redshift

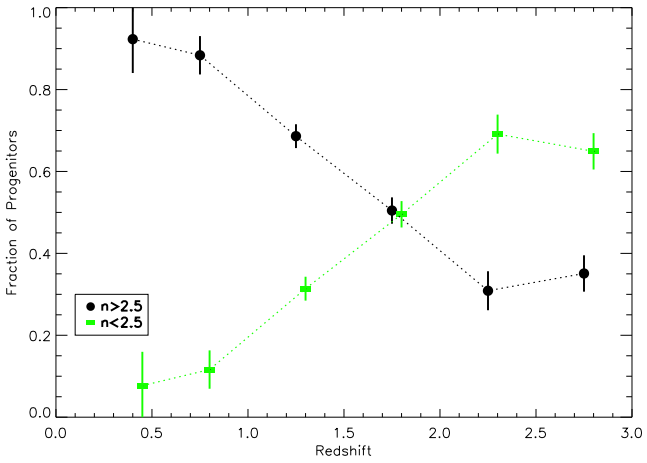

(a)

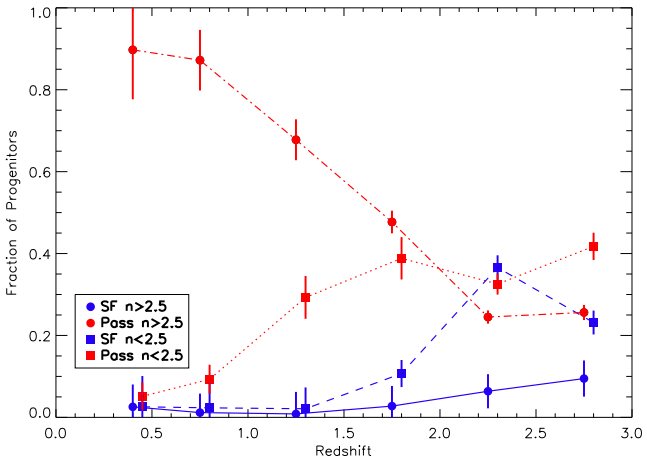

(b)

Figure 10. Fraction of the progenitors of local massive galaxies with high ($n > 2.5$) and low ($n < 2.5$) Sérsic indices. Figure (a) show the evolution of the whole progenitor sample with, green rectangles showing the fraction of progenitors with low Sérsic index and, black circles showing progenitors with high Sérsic light profiles as a function of redshift. Error bars are derived using Monte Carlo analysis. Figure (b) shows the high and low Sérsic populations split into star-forming and passive systems.

with low Sérsic indices also display disturbed morphologies when examined using visual classification. These studies also showed that the number of galaxies with disturbed visual morphologies increases dramatically with redshift, with ∼40 per cent of massive galaxies showing a disturbed morphology at $z = 3$. This increase in the number of galaxies with disturbed morphologies could be linked to the increase in the importance of major mergers with redshift shown in e.g. Bluck et al. (2012), Ownsworth et al. (2014), Conselice et al. (2003, 2011), and Conselice, Yang & Bluck (2009).

Therefore, using just the Sérsic profile information we cannot determine if the progenitor galaxy population we present here are true discs or disturbed galaxies. Examining the asymmetries of our galaxies (e.g. CAS; Conselice 2006a) shows that a large fraction of these systems are indeed undergoing mergers (see Mortlock et al. 2013 for more discussion). From the limited number of galaxies at these masses studied in Mortlock et al. (2013) we know that at $z > 2.75$ around 60 per cent of these galaxies are peculiar with

the remainder having a visual morphology of smooth elliptical like systems. The fact that these galaxies visually do not have discs shows that they are not the equivalent of lower redshift discs and therefore have a different formation history.

Also from Fig. 10(a) we find that the redshift where the progenitor galaxies transition into the high Sérsic index dominated population we see in the local Universe is between $1.5 < z < 2.0$. This is in agreement with previous studies which examine the morphological change of galaxies with similar stellar masses as our sample (e.g. Mortlock et al. 2013). Mortlock et al. (2013) show that this is also the redshift range where peculiar galaxies transition into normal ellipticals and spirals. We see the same for our galaxies but within a transition from low to high Sérsic index systems.

We further divide the high and low Sérsic progenitor samples into star-forming and passive systems using our *UVJ* selection and present the results in Fig. 10(b). This figure shows the clear dominance at $z < 1.7$ of the passive high Sérsic index systems that we associate with massive galaxies in the local Universe. The population of high Sérsic index galaxies is, at all redshifts examined in this study, dominated by the passive population. The star-forming and high Sérsic index systems are the least abundant at $z = 3.0$, only constituting 9 ± 3 per cent of the total progenitor population at this redshift.

Examining the low Sérsic index systems we find that these objects are dominated at almost all redshifts by passive systems, much like the high Sérsic index population. At $z = 2.5$, 41 ± 4 per cent of the progenitor galaxies are passive and have low Sérsic indices, and 23 ± 3 per cent of the progenitor galaxies are star forming and have low Sérsic indices. This result implies that passive low Sérsic index systems out number star-forming low Sérsic index systems by nearly a factor of 2 within the progenitor massive galaxy population. This result is surprising as the morphologies that constitute the low Sérsic index population are generally thought to be star forming. However, this result is in agreement with recent work by Bruce et al. (2014) using two component light profile fitting which has shown that a large fraction, $\sim$38 per cent of passive massive galaxies at $z > 1.5$ are disc-like dominant systems.

We also find in our previous work on this sample (Ownsworth et al. 2014) that the size evolution for this population evolves by a factor of at most 2 between $0.5 < z < 3$. This is much less than the factor of 5 or so found for a mass-selected sample over the same redshift range (e.g. Buitrago et al. 2008). However, there is still an evolution in size that must come about from something other than finding the wrong progenitors of low-redshift massive galaxies.

A clue to this is that the dominant population at high-z for this sample are galaxies with low Sérsic indices, which become larger at higher redshifts. Also, as we discuss above, the dominant type of galaxy in this selection at $z \sim 3$ are passive systems. Therefore this shows that star formation is unlikely to be the cause of the increased sizes and higher Sérsic indices as time goes on (see also Ownsworth et al. 2012). The most likely explanation for this is minor mergers which occur in about the right quantity to account for the evolution seen (e.g. Bluck et al. 2012). The fact that there is a decoupling between when galaxies become passive (which occurs at $z > 1$) and this structural evolution implies that a dynamical effect, such as these minor mergers, are the cause of the continued structural evolution at $z < 1$.

Furthermore, we see a strong correlation between the galaxies which have a high Sérsic index and those that are passive. This demonstrates that passivity and structure are highly correlated, and that most likely the formation of a galaxy into a concentrated profile leads to the shutting down of star formation.

4 SUMMARY

In this paper, we present a study of the evolution of the properties of galaxies constituting a constant number density selected sample over the redshift range of $0.3 < z < 3.0$. Our main sample are galaxies selected by a constant number density of $n = 10^{-4}$ Mpc^{-3} which ranges from galaxies with stellar masses $M_* = 10^{10.54}$ M$_\odot$ at $z = 2.75$ to $M_* = 10^{11.24}$ M$_\odot$ at $z = 0.3$. We examine the evolution of colour, location on the colour–stellar mass diagram, passivity and, structural parameters. We find the following principle results.

(i) We find that the average $U - V$ and $V - J$ colours of the progenitors of local massive galaxies have been located within the *UVJ* defined passive region since at least $z = 3.0$. However the progenitors that are classified as star forming have a large scatter in both colours, and in some cases show redder colours than the passive galaxies at the same epoch. When we examine these galaxies using the colour–stellar mass diagram we also find that the average progenitor of local massive galaxies has not lived on the blue cloud since $z = 3.0$. Using stellar population models we find that the progenitor galaxies which are passive have old stellar ages (age >5 Gyr) and appear to show hints that they have been passively evolving since at least $z = 4$.

(ii) We examine how the progenitor population becomes the passive population we see today over this redshift range. We find that the passive fraction of the progenitor galaxies undergoes significant evolution from $z = 3.0$, increasing from 27 per cent at $z = 3.0$ (from our fit, 50 per cent observed at $z = 2.5$) to 94 ± 8 per cent at $z = 0.3$. This implies that over half of the population of the progenitors of local massive galaxies have already stopped forming stars by $z = 3.0$. Also the star formation density of the progenitors shows signs of galaxy downsizing, with galaxies selected in a given number density becoming passive earlier than those selected at higher densities.

(iii) The morphological evolution of the progenitor galaxies is probed using the evolution of the Sérsic indices within the sample. We find that these galaxies are dominated at high redshifts by low Sérsic index ($n < 2.5$) light profiles and evolve to become high Sérsic index ($n > 2.5$) dominated objects by $z = 1.7$. We further split the high and low Sérsic populations into star-forming and passive systems. We find that passive high Sérsic index systems are the most abundant objects at $z < 1.7$, equivalent to their descendants at $z \sim 0$. There exists a small population of star-forming high Sérsic index objects at high redshift but they rapidly decrease towards low redshift. We also find that 41 ± 4 per cent of the population within the highest redshift bin are passive low Sérsic index objects. This could imply that a significant proportion of the progenitors of massive galaxies were passive disc-like systems at early times. However, this low Sérsic index trend could be driven by the increase in the abundance of morphologically disturbed systems at higher redshifts.

We previously investigated the size evolution of the constant number density selected sample using no passivity cuts and find that the sizes of the progenitors of massive galaxies range from a factor of 1.8 to 1.2 smaller than local early-type galaxies of similar mass over $0.5 < z < 3$ (Ownsworth et al. 2014). This is smaller than previous studies have found, quoting size evolution factors of 2–4.

However, this does show that galaxy evolution is occurring within the galaxy population selected to be as close as possible the same systems over redshifts. Previous studies were limited in making this conclusion based on using a constant mass selection whereby there

is significant precursor bias contamination to the level of 95 per cent since $z < 1$.

To further this work, especially when probing high number densities, or lower mass objects, or to extend to $z > 3$ will require larger and deeper surveys. Future telescopes such as *JWST*, E-ELT and *Euclid* will be able to push these trends out to higher redshifts and be able to investigate the full history of local massive galaxies. However, in all surveys any future conclusions about galaxy evolution must use a number density selected sample as outlined in this paper, or else will have a significant and catastrophic precursor bias.

ACKNOWLEDGEMENTS

We thank the anonymous referee for critical and useful comments which improved this paper significantly. We also thank the UDS team for their support and work on this survey and assistance on this paper. We acknowledge funding from the STFC and the Leverhulme trust for supporting this work. AM acknowledges funding from the STFC and a European Research Council Consolidator Grant (PI R. McLure).

REFERENCES

Baldry I. K., Glazebrook K., Brinkmann J., Ivezić Ž., Lupton R. H., Nichol R. C., Szalay A. S., 2004, ApJ, 600, 681
Baldry I. K., Balogh M. L., Bower R. G., Glazebrook K., Nichol R. C., Bamford S. P., Budavari T., 2006, MNRAS, 373, 469
Barden M. et al., 2005, ApJ, 635, 959
Barden M., Häußler B., Peng C. Y., McIntosh D. H., Guo Y., 2012, MNRAS, 422, 449
Bell E. F., McIntosh D. H., Katz N., Weinberg M. D., 2003, ApJS, 149, 289
Bluck A. F. L., Conselice C. J., Buitrago F., Grutzbauch R., Hoyos C., Mortlock A., Bauer A., 2012, ApJ, 747, 34
Bower R. G., Lucey J. R., Ellis R. S., 1992, MNRAS, 254, 601
Brammer G. B., van Dokkum P. G., Coppi P., 2008, ApJ, 686, 1503
Brammer G. et al., 2011, ApJ, 739, 24
Bruce V. A. et al., 2014, MNRAS, 444, 1001
Bruzual G., Charlot S., 2003, MNRAS, 344, 1000
Buitrago F., Trujillo I., Conselice C., Bouwens R., Dickinson M., Yan H., 2008, ApJ, 687, 61
Buitrago F., Trujillo I., Conselice C. J., Häußler B., 2013, MNRAS, 428, 1460
Bundy K., Ellis R., Conselice C. J., 2005, ApJ, 625, 621
Bundy K. et al., 2006, ApJ, 651, 120
Calzetti D., Kinney A. L., Storchi-Bergmann T., 1994, AJ, 429, 582
Charlot S., Fall S. M., 2000, ApJ, 539, 718
Chuter R. W. et al., 2011, MNRAS, 413, 1678
Cole S. et al., 2001, MNRAS, 326, 255
Conselice C. J., 2006a, MNRAS, 373, 1389
Conselice C. J., 2006b, ApJ, 638, 686
Conselice C. J., Bershady M. A., Dickinson M., Papovich C., 2003, AJ, 126, 1183
Conselice C. J. et al., 2007, MNRAS, 381, 962
Conselice C. J., Rajgor S., Myers R., 2008, MNRAS, 386, 909
Conselice C. J., Yang C., Bluck A. F. L., 2009, MNRAS, 394, 1956
Conselice C. J., Bluck A. F. L., Ravindranath S., Mortlock A., Koekemoer A. M., Buitrago F., Grützbauch R., Penny S. J., 2011, MNRAS, 417, 2770
Conselice C. J., Mortlock A., Bluck A. F. L., Grützbauch R., Duncan K., 2013, MNRAS, 430, 1051
Daddi E., Cimatti A., Renzini A., Fontana A., Mignoli M., Pozzetti L., Tozzi P., Zamorani G., 2004, ApJ, 617, 746
Daddi E. et al., 2007, ApJ, 670, 156
Duncan K. et al., 2014, MNRAS, 444, 2960
Fischera J., Dopita M., 2005, ApJ, 619, 340
Furusawa H., Kosugi G., Akiyama M., Takata T., Sekiguchi K., Furusawa J., 2008, 399, 131
Gallazzi A., Charlot S., Brinchmann J., White S. D. M., Tremonti C. A., 2005, MNRAS, 362, 41
Grogin N. A. et al., 2011, ApJS, 197, 35
Grützbauch R. et al., 2011, MNRAS, 418, 938
Hartley W. G. et al., 2013, MNRAS, 431, 3045
Hartley W. G., Conselice C. J., Mortlock A., Foucaud S., Simpson C., 2015, MNRAS, 451, 1613
Hopkins A. M., Beacom J. F., 2006, ApJ, 651, 142
Ilbert O. et al., 2013, A&A, 556, 55
Kauffmann G. et al., 2003, MNRAS, 341, 54
Kaviraj S. et al., 2013, MNRAS, 428, 925
Kennicutt R. C., Jr, 1983, ApJ, 272, 54
Kennicutt R. C., Jr, 1998, ARA&A, 36, 189
Koekemoer A. M. et al., 2011, ApJS, 197, 36
Lani C. et al., 2013, MNRAS, 435, 207
Lawrence A. et al., 2007, MNRAS, 379, 1599
Leja J., van Dokkum P., Franx M., 2013, ApJ, 766, 33
McIntosh D. H. et al., 2005, ApJ, 632, 191
McLure R. J. et al., 2013, MNRAS, 432, 2696
Marchesini D. et al., 2014, ApJ, 794, 65
Margalef-Bentabol et al. 2016, submitted
Meurer G. R., Heckman T. M., Calzetti D., 1999, ApJ, 521, 64
Mortlock A. et al., 2013, MNRAS, 433, 1185
Mortlock A., Conselice C. J., Bluck A. F. L., Bauer A. E., Grutzbauch R., Buitrago F., Ownsworth J., 2011, MNRAS, 413, 2845
Mortlock A. et al., 2015, MNRAS, 447, 2
Mundy C. J., Conselice C. J., Ownsworth J. R., 2015, MNRAS, 450, 3696
Muzzin A. et al., 2013, ApJ, 777, 18
Ownsworth J. R., Conselice C. J., Mortlock A., Hartley W. G., Buitrago F., 2012, MNRAS, 426, 764
Ownsworth J. R., Conselice C. J., Mortlock A., Hartley W. G., Almaini O., Duncan K., Mundy C. J., 2014, MNRAS, 445, 2198
Papovich C., Finkelstein S. L., Ferguson H. C., Lotz J. M., Giavalisco M., 2011, MNRAS, 412, 1123
Papovich C. et al., 2015, MNRAS, 803, 26
Patel S. G. et al., 2013, ApJ, 766, 15
Peng Y. et al., 2010, ApJ, 721, 193
Pozzetti L. et al., 2010, A&A, 523, A13
Prevot M. L., Lequeux J., Prevot L., Maurice E., Rocca-Volmerange B., 1984, A&A, 132, 389
Quadri R. F., Williams R. J., 2010, ApJ, 725, 794
Renzini A., 2006, ARA&A, 44, 141
Sérsic J. L., 1968, Atlas de Galaxias Australes. Observatorio Astronomico, Cordoba, Argentina
Shen S., Mo H. J., White S. D. M., Blanton M. R., Kauffmann G., Voges W., Brinkmann J., Csabai I., 2003, MNRAS, 343, 978
Simpson C. et al., 2006, MNRAS, 372, 741
Taylor E. N. et al., 2015, MNRAS, 446, 2144
Taylor-Mager V. A., Conselice C. J., Windhorst R. A., Jansen R. A., 2007, ApJ, 569, 162
Trujillo I., Conselice C. J., Bundy K., Cooper M. C., Eisenhardt P., Ellis R., 2007, MNRAS, 382, 109
Ueda Y. et al., 2008, ApJS, 179, 124
van der Wel A. et al., 2012, ApJS, 203, 24
Whitaker K. E., Kriek M., van Dokkum P. G., Bezanson R., Brammer G., Franx M., Labbé I., 2012, ApJ, 745, 179
Wilkinson et al. 2016, submitted
Williams R. J., Quadri R. F., Franx M., van Dokkum P., Labbé I., 2009, ApJ, 691, 1879

APPENDIX A

In the appendix we show the *UVJ* colours of a few other number density selections to compare with the nominal one at

$n = 10^{-4}$ Mpc^{-3}. We investigate this to determine how our results depend upon the selection method using other number densities.

The other number densities that we investigate are: $n = 10^{-5}$ Mpc^{-3} (Figs A1 and A3) and $n = 3 \times 10^{-4}$ Mpc^{-3} (Figs A2 and A4). Both of these number density selections show similar behaviour as the $n = 10^{-4}$ Mpc^{-3} sample (Section 3.1). The only difference is that we see a signature of downsizing, whereby the lower number densities, tracing higher mass galaxies, become a homogeneous red/passive population earlier than galaxies selected at higher number densities, or lower mass galaxies (see main body of paper for details).

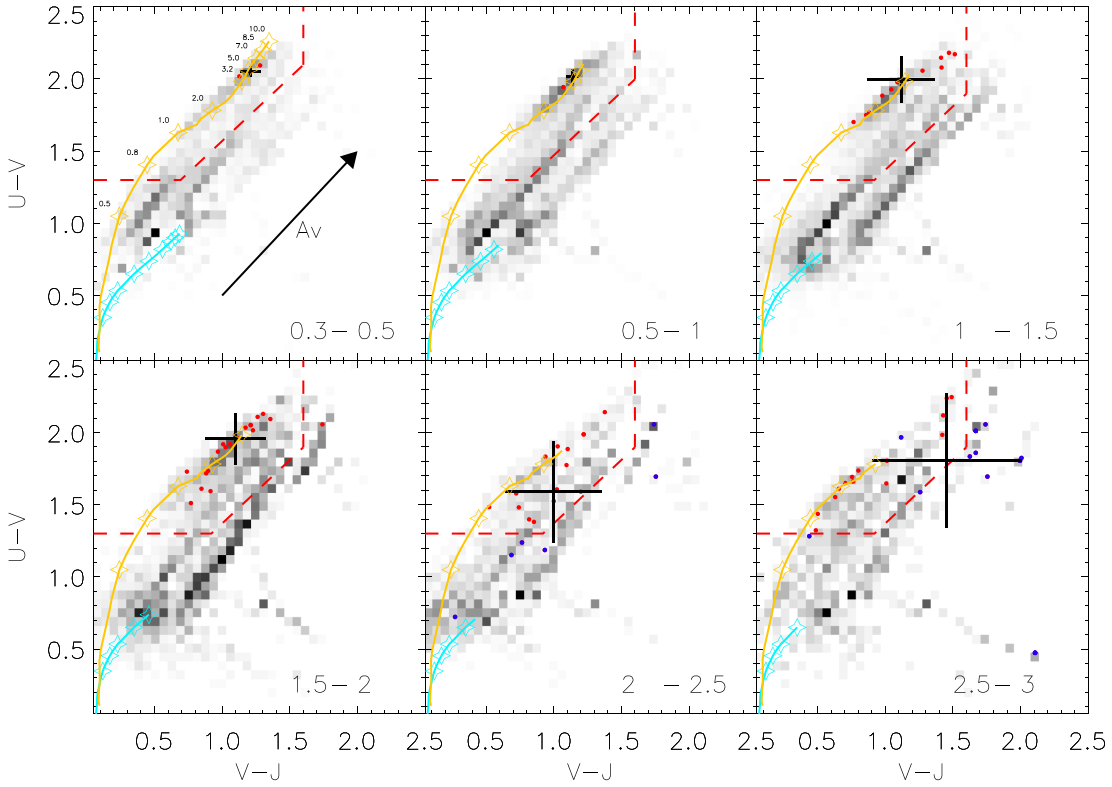

Figure A1. Rest-frame $U - V$ versus $V - J$ diagram in redshift bins between $z = 0.3$ and 3.0 for the constant number density selected sample with $n = 10^{-5}$ Mpc^{-3}, corresponding to a mass limit of log $M_* \sim 11.59$ at $z \sim 0.3$. The red dashed line denotes the *UVJ* passive selection. Red circles show the progenitors of massive galaxies that are selected as passive via the *UVJ* method. Blue circles show the progenitors of massive galaxies that are selected as star forming via the *UVJ* method and 24 μm criteria. The black cross shows the median colour and standard deviation for the progenitor sample in each redshift bin. The colour evolution tracks from Bruzual & Charlot (2003) SSP models are also shown. The light blue line shows a constant star formation history with no dust and the yellow line shows an exponentially declining star formation history with $\tau = 0.1$ Gyr (see Fig. 2). The open stars represent model colours at the specified ages, given in Gyr. The colour evolution tracks are plotted up to the age of the Universe in each redshift bin.

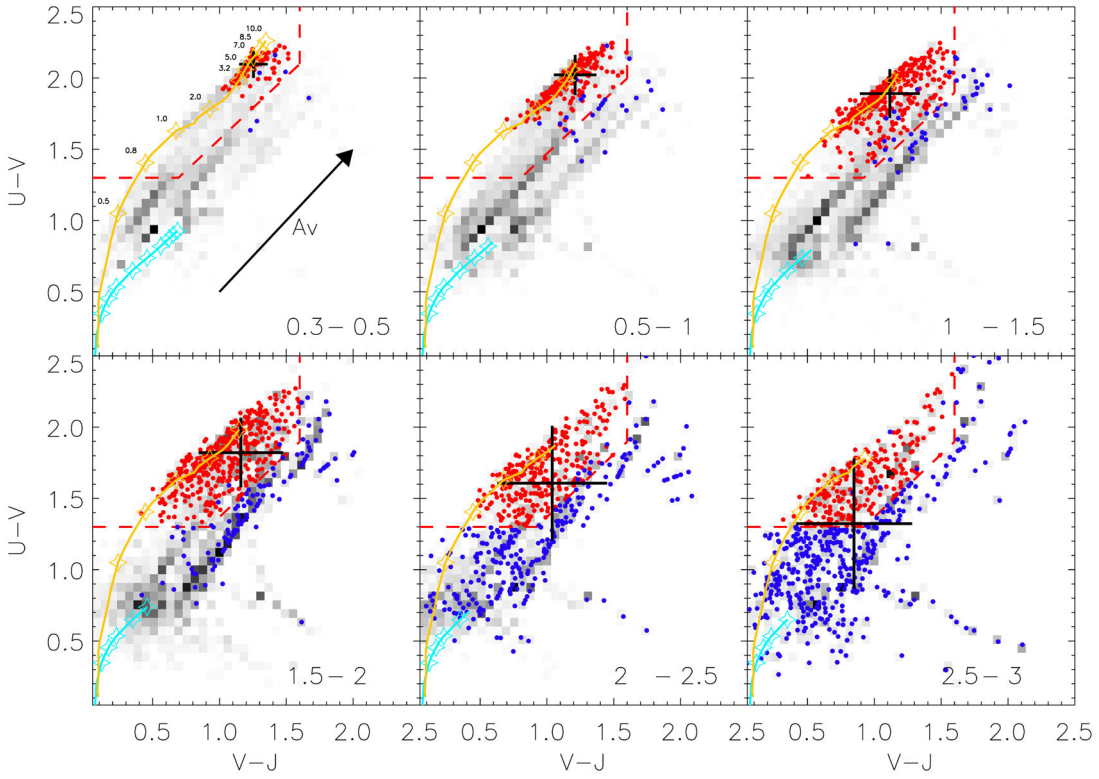

Figure A2. Rest-frame $U - V$ versus $V - J$ diagram in redshift bins between $z = 0.3$ and 3.0 for the constant number density selected sample with $n = 3 \times 10^{-4}$ Mpc^{-3}, corresponding to a mass limit of log $M_* \sim 10.93$ at $z \sim 0.3$. The red dashed line denotes the *UVJ* passive selection. Red circles show the progenitors of massive galaxies that are selected as passive via the *UVJ* method. Blue circles show the progenitors of massive galaxies that are selected as star forming via the *UVJ* method and 24 μm criteria. The black cross shows the median colour and standard deviation for the progenitor sample in each redshift bin. The colour evolution tracks from Bruzual & Charlot (2003) SSP models are also shown. The light blue line shows a constant star formation history with no dust and the yellow line shows an exponentially declining star formation history with $\tau = 0.1$ Gyr (see Fig. 2). The open stars represent model colours at the specified ages, given in Gyr. The colour evolution tracks are plotted up to the age of the Universe in each redshift bin.

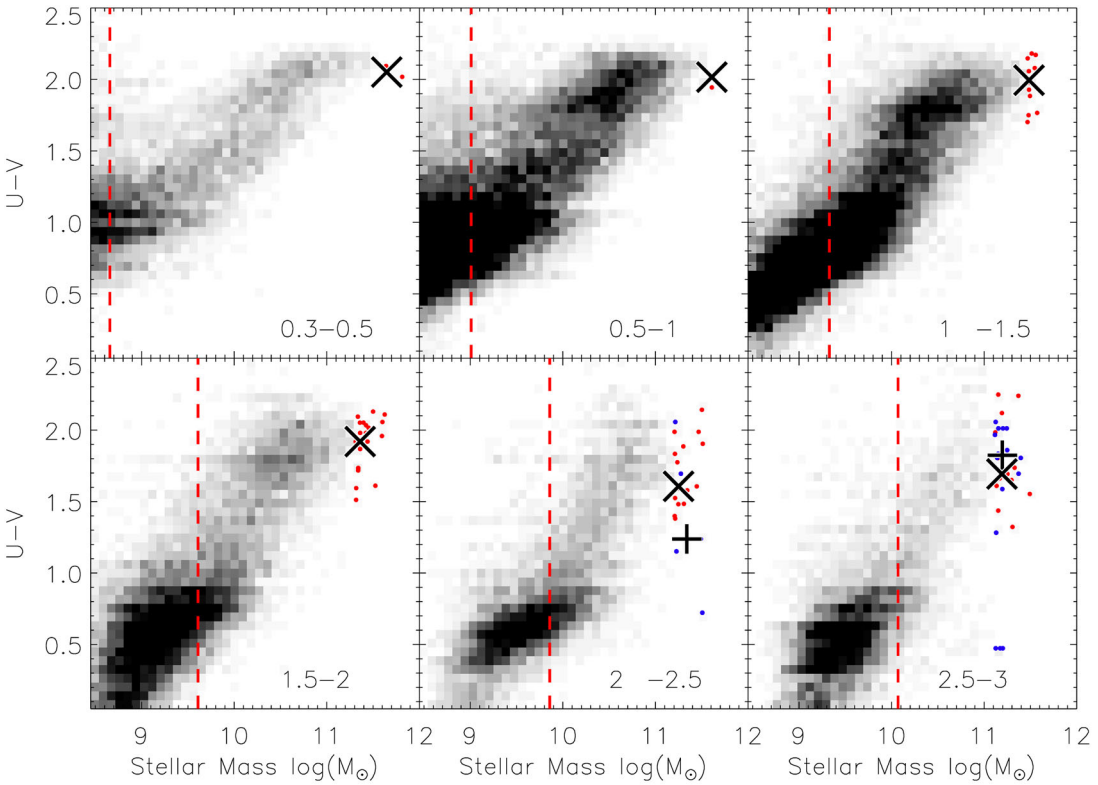

Figure A3. Stellar mass versus rest-frame $U - V$ colour for all galaxies selected via the constant number density selected sample with $n = 10^{-5}$ Mpc^{-3}. The red circles show the progenitors of massive galaxies that are selected as passive via the *UVJ* method. The blue circles show the progenitors of massive galaxies that are selected as star forming via the *UVJ* method. The black 'X' shows the median $U - V$ colour for the passive population and the black plus sign shows the median $U - V$ colour for the star-forming population. The grey-scale shows the whole UDS galaxy sample within each redshift bin. The red dashed line shows the 95 per cent stellar mass completeness limit, such that the sample in each plot is complete to the right of this line.

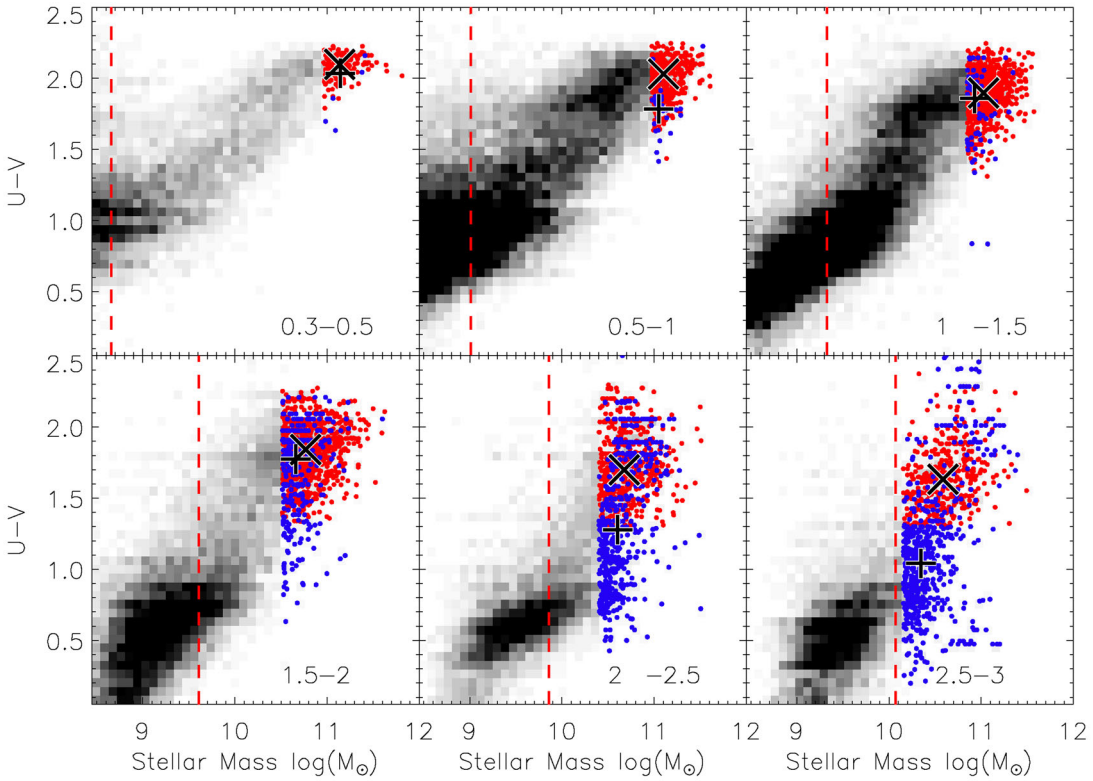

Figure A4. Stellar mass versus rest-frame $U - V$ colour for all galaxies selected via the constant number density selected sample with $n = 3 \times 10^{-4}$ Mpc^{-3}. The red circles show the progenitors of massive galaxies that are selected as passive via the *UVJ* method. The blue circles show the progenitors of massive galaxies that are selected as star forming via the *UVJ* method. The black 'X' shows the median $U - V$ colour for the passive population and the black plus sign shows the median $U - V$ colour for the star-forming population. The grey-scale shows the whole UDS galaxy sample within each redshift bin. The red dashed line shows the 95 per cent stellar mass completeness limit.

This paper has been typeset from a TEX/LATEX file prepared by the author.